David Taylor Research Center
Bethesda, MD 20084–5000

AD-A226 382

DTRC–SME–90/18 July 1990

Ship Materials Engineering Department
Research & Development Report

Procedure for Drop Tower Testing of Shallow Cracked Single Edge Notched Bend Specimens

by
M.T. Kirk
J.P. Waskey
R.H. Dodds, Jr.

DTRC–SME–90/18 Procedure for Drop Tower Testing of Shallow Cracked Single Edge Notched Bend Specimens

MAJOR DTRC TECHNICAL COMPONENTS

CODE 011 DIRECTOR OF TECHNOLOGY, PLANS AND ASSESSMENT

12 SHIP SYSTEMS INTEGRATION DEPARTMENT

14 SHIP ELECTROMAGNETIC SIGNATURES DEPARTMENT

15 SHIP HYDROMECHANICS DEPARTMENT

16 AVIATION DEPARTMENT

17 SHIP STRUCTURES AND PROTECTION DEPARTMENT

18 COMPUTATION, MATHEMATICS & LOGISTICS DEPARTMENT

19 SHIP ACOUSTICS DEPARTMENT

27 PROPULSION AND AUXILIARY SYSTEMS DEPARTMENT

28 SHIP MATERIALS ENGINEERING DEPARTMENT

DTRC ISSUES THREE TYPES OF REPORTS:

1. **DTRC reports, a formal series,** contain information of permanent technical value. They carry a consecutive numerical identification regardless of their classification or the originating department.

2. **Departmental reports, a semiformal series,** contain information of a preliminary, temporary, or proprietary nature or of limited interest or significance. They carry a departmental alphanumerical identification.

3. **Technical memoranda, an informal series,** contain technical documentation of limited use and interest. They are primarily working papers intended for internal use. They carry an identifying number which indicates their type and the numerical code of the originating department. Any distribution outside DTRC must be approved by the head of the originating department on a case-by-case basis.

NDW-DTNSRDC 5602 51 (Rev 2-88)

REPORT DOCUMENTATION PAGE

1a. REPORT SECURITY CLASSIFICATION Unclassified	1b. RESTRICTIVE MARKINGS
2a. SECURITY CLASSIFICATION AUTHORITY	3. DISTRIBUTION/AVAILABILITY OF REPORT Approved for public release: distribution is unlimited.
2b. DECLASSIFICATION/DOWNGRADING SCHEDULE	
4. PERFORMING ORGANIZATION REPORT NUMBER(S) DTRC-SME-90/18	5. MONITORING ORGANIZATION REPORT NUMBER(S)
6a. NAME OF PERFORMING ORGANIZATION David Taylor Research Center 6b. OFFICE SYMBOL (If applicable) Code 2814	7a. NAME OF MONITORING ORGANIZATION
6c. ADDRESS (City, State, and ZIP Code) Annapolis, MD 21402	7b. ADDRESS (City, State, and ZIP Code)
8a. NAME OF FUNDING/SPONSORING ORGANIZATION David Taylor Research Center 8b. OFFICE SYMBOL (If applicable) Code 011.5	9. PROCUREMENT INSTRUMENT IDENTIFICATION NUMBER
8c. ADDRESS (City, State, and ZIP Code) Bethesda, MD 20084-5000	10. SOURCE OF FUNDING NUMBERS PROGRAM ELEMENT NO.: 62234N PROJECT NO.: TASK NO.: RS345S50 WORK UNIT ACCESSION NO.: DN507603

11. TITLE (Include Security Classification)

A Procedure for Drop Tower Testing of Shallow Cracked Single Edge Notched Bend Specimens

12. PERSONAL AUTHOR(S)

M.T. Kirk, J.P. Waskey, and R.H. Dodds, Jr.

13a. TYPE OF REPORT	13b. TIME COVERED	14. DATE OF REPORT (YEAR, MONTH, DAY)	15. PAGE COUNT
Research and Development	FROM 6/89 TO 2/90	July 1990	

16. SUPPLEMENTARY NOTATION

1-2814-950-30, 50FR3/2

17. COSATI CODES			18. SUBJECT TERMS (Continue on reverse if necessary and identify by block number)
FIELD	GROUP	SUB-GROUP	Shallow crack, Impact testing, J-Integral, Initiation fracture toughness Experimental procedure

19. ABSTRACT (Continue on reverse if necessary and identify by block number)

Under predictions of the reserve capacity of structures against fracture often result from the use of conventional initiation fracture toughness values (e.g., J_{IC}, δc) measured using deeply cracked bend specimens. Conversely, favorable comparisons between predictions and structural fracture behavior have been reported when the predictions are based on toughness values measured in such a manner that the crack tip constraint and the loading rate closely match those experienced in service. As a result, considerable attention has recently been paid to the elevated fracture initiation resistance of cracks shallower than the 0.45 to 0.75 a/W used in standardized tests. However, standard procedures for estimating the fracture initiation resistance of shallow cracks, particularly at the high loading rates characteristic of certain severe service conditions, have yet to be developed. In this investigation, techniques useful for estimating the load, load line displacement, and the onset of crack extension during impact tests of single edge notched bend specimens having shallow fatigue cracks ($a/W \approx 0.1$) were developed and validated. The bending stress distribution across the specimen midway between the support and loading points, determined based on strain measurements and a uniaxial stress-strain relationship, was used to estimate the load imparted to the specimen by the impactor. Load line displacement was estimated using four non-contacting transducers positioned along the underside of the bend specimen, while the onset of crack extension was inferred from strain readings taken from the elastically loaded region behind the fatigue crack tip. The applicability of these procedures was demonstrated at an impact loading rate of 4.88 m/s, while control experiments at quasi-static loading rates were used to demonstrate the accuracy of these new procedures for alloy steels of both low and high strain hardening capacity.

20. DISTRIBUTION/AVAILABILITY OF ABSTRACT	21. ABSTRACT SECURITY CLASSIFICATION
☒ UNCLASSIFIED/UNLIMITED ☐ SAME AS RPT ☐ DTIC USERS	Unclassified

22a. NAME OF RESPONSIBLE INDIVIDUAL	22b. TELEPHONE (Include Area Code)	22c. OFFICE SYMBOL
M. T. Kirk	(301) 267-3755	Code 2814

TABLE OF CONTENTS

LIST OF TABLES

LIST OF FIGURES

ABSTRACT

Under predictions of the reserve capacity of structures against fracture often result from the use of conventional initiation fracture toughness values (e.g. J_{Ic}, δ_c) measured using deeply cracked bend specimens. Conversely, favorable comparisons between predictions and structural fracture behavior have been reported when the predictions are based on toughness values measured in such a manner that the crack tip constraint and the loading rate closely match those experienced in service. As a result, considerable attention has recently been paid to the elevated fracture initiation resistance of cracks shallower than the 0.45 to 0.75 a/W used in standardized tests. However, standard procedures for estimating the fracture initiation resistance of shallow cracks, particularly at the high loading rates characteristic of certain severe service conditions, have yet to be developed. In this investigation, techniques useful for estimating the load, load line displacement, and the onset of crack extension during impact tests of single edge notched bend specimens having shallow fatigue cracks ($a/W \approx 0.1$) were developed and validated. The bending stress distribution across the specimen midway between the support and loading points, determined based on strain measurements and a uniaxial stress-strain relationship, was used to estimate the load imparted to the specimen by the impactor. Load line displacement was estimated using four non-contacting transducers positioned along the underside of the bend specimen, while the onset of crack extension was inferred from strain readings taken from the elastically loaded region behind the fatigue crack tip. The applicability of these procedures was demonstrated at an impact loading rate of 4.88 m/s, while control experiments at quasi-static loading rates were used to demonstrate the accuracy of these new procedures for alloy steels of both low and high strain hardening capacity.

ADMINISTRATIVE INFORMATION

This report was prepared as part of the Surface Ship and Submarine Materials Block under the sponsorship of I. Caplan (DTRC 011.5). The work of the first and second authors was performed at this Center under Program Element 62234N, Task Area RS345S50, Work Unit 1-2814-950-30; the work was supervised by of T.W. Montemarano. The work of the third author was performed under contract N61533-88-C-0035 to the University of Illinois. This report satisfies milestone 50FR3/2.

ACKNOWLEDGMENTS

The authors are pleased to acknowledge the able technical assistance rendered by M. Keppell, S. Mikalac, and J. Hein. Additionally, the many helpful discussions with M.G. Vassilaros and E.M. Hackett are gratefully acknowledged. E.M. Hackett is to be especially thanked for his kind provision of the tensile data for the low hardening material.

INTRODUCTION

The deep cracks used in standard fracture toughness test specimens (a_o/W = 0.45 to 0.75) maximize the crack tip stress triaxiality, thereby insuring the measurement of a lower bound, geometry independent fracture toughness value. However, use of such lower bound values in structural fracture integrity assessments often leads to significant under predictions of the reserve capacity against fracture [1,2] due to a mismatch between the degree of triaxial plane-strain constraint in the test specimen and in the structure. Accordingly, there has recently been considerable attention paid to the elevated fracture initiation resistance characteristic of cracks shallower than a normalized crack depth (a/W) of 0.45 to 0.75 as used in standard test specimens [3-9]. While it is commonly recognized that a geometry independent toughness value has been sacrificed in the process, the improved accuracy of the structural failure predictions that can be achieved using toughness values measured with specimens having shallow cracks [1,2] provides a useful engineering tool.

The preceding comments suggest that the accuracy of a structural fracture integrity assessment depends on matching the crack depth in the fracture toughness specimen to the crack depth in the structure. For ferritic steels, there is an additional requirement that the loading rate applied to the fracture specimen be similar to that experienced in service, due to the dependence of fracture toughness, fracture mode, and flow properties on the rate of load application for these steels. Accordingly, this report presents

a procedure for determining the initiation fracture toughness of impact loaded ferritic materials having shallow initial crack depths ($a_o/W \approx 0.1$). The scope of this procedure was limited to loading rates below those at which the equations used to interpret the experimental data need to account for kinetic energy terms.

The value of the J-integral at crack initiation in a shallow cracked bend specimen can be estimated by the following equation proposed by Sumpter [8]:

$$J_i = \frac{K^2 \cdot (1 - \nu^2)}{E} + \frac{\eta_p}{B \cdot b} \cdot \int_0^{\Delta_{pLL}{}^i} P \, d\Delta_{pLL} \qquad (1)$$

where

K = linear elastic stress intensity factor calculated from the applied load at crack initiation;
ν = Poisson's ratio;
E = Young's modulus;
η_p = $0.32 + 12.0(a/W) - 49.5(a/W)^2 + 99.8(a/W)^3$ for $a/W < 0.282$;
= 2.0 for $a/W \geq 0.282$;
a = crack depth;
W = specimen width;
Δ_{pLL} = plastic component of load line displacement;
P = load;
$\Delta_{pLL}{}^i$ = plastic component of load line displacement at crack initiation;
B = specimen thickness; and
b = specimen remaining ligament.

This equation indicates that measurements of load, load line displacement, and detection of crack initiation are required to evaluate J_i. In this investigation, procedures useful for measuring these quantities during impact experiments on single edge notch bend, SE(B), specimens having shallow through cracks were developed and validated.

APPROACH

To demonstrate the validity of candidate procedures for dynamic load, load line displacement, and crack initiation measurements, the following requirements must be fulfilled:

1. the accuracy of the procedures must be demonstrated by comparison to control measurements,

2. it must be demonstrated that the transducers used to make the measurements have an acceptable frequency response for the impact loading events of interest, and

3. it must be demonstrated that kinetic energy terms can be ignored in the data analysis without undue error.

To this end, the following steps were taken:

1. SE(B) experiments at quasi-static loading rates were performed so that the experimental load and load line displacement values estimated using the candidate procedures for impact loading could be compared to control measurements accurately made at a slower loading rate.

2. SE(B) experiments at impact loading rates were performed to demonstrate that the data required for the candidate load and load line displacement estimation procedures could be obtained and analyzed, and that the transducers used to make these measurements had an adequate frequency response. Additionally, data from these experiments was used to demonstrate that an analysis procedure which ignores kinetic energy terms had acceptable accuracy.

3. A series of impact SE(B) experiments was performed, where each specimen experienced a different total load line displacement so as to achieve different amounts of stable crack extension from the fatigue precrack. The results of these experiments were used to validate the candidate procedure for determining the time at which crack initiation occurred during impact loading.

Specimens for experiments performed as part of the first step were

prepared from steel plates with both low strain hardening (Ultimate / Yield Strength (U/Y) ratio = 1.15) and high strain hardening (U/Y Ratio = 1.81) capacities, while experiments for the second and third steps were performed using only the low hardening steel. The low strain hardening steel was a 64 mm thick plate of HY-100, while the high strain hardening steel was a 127 mm thick plate of ASTM A515 Grade 70. The transverse tensile properties of these two steels at both quasi-static and impact loading rates are reported in Table 1. Square cross section (50.8mm x 50.8mm) SE(B) specimens were used for all tests reported herein. The SE(B) specimens were taken in the T-S orientation; they had an initial a/W of approximately 0.1 and were tested with a span to width ratio of 4:1.

EXPERIMENTAL PROCEDURES

SE(B) TESTING

Quasi-static tests were performed in a screw driven testing machine at a constant displacement rate until the desired displacement was achieved. Dynamic fracture tests were conducted in a drop tower with the load applied by a free-falling crosshead loaded with 669 kg of lead weights. The crosshead was dropped from a height of 1.22 m to achieve an initial displacement rate of 4.88 m/s and was arrested onto rigid stops after impacting and displacing the specimen by a prescribed amount. The SE(B) specimens were supported on two hardened anvils having same width as the specimen. A pyramidal aluminum absorber (base of 25.4mm x 38.1 mm, height at the apex of 25.4 mm, and a hardness of 22 HB 500) was placed between the falling cross head and the specimen. The impact flattened the absorber to a pancake approximately 2.5 mm thick. By flattening in this way, the absorber served as a deformable link between the specimen and the tup, allowing load to be transferred smoothly to the specimen without the erratic load excursions ("ringing") which typically occur due to loss of contact between the loading tup and the specimen. This technique has been employed previously by Madison and Irwin [10] and by Joyce and Hackett [11] using different absorber configurations.

Load Measurement

Load was measured by an array of six individual quarter bridge strain gages. These gages were positioned as illustrated in Figure 1 to measure the bending strains along the quarter span position. Load was calculated from these bending strains using the following equation, which was derived using beam theory based on static equilibrium requirements, the boundary conditions, the position of the strain gage array relative to the loading points, and the assumption that plane sections remain plane:

$$P = \frac{-8 \cdot B}{S} \cdot \int_W \sigma(\epsilon) \cdot y \, dy \qquad (2a)$$

where

$\sigma(\epsilon)$ = bending stress along quarter span based on measured strains;
W = specimen width;
S = span between supports = $4 \cdot W$; and
y = distance from neutral axis (positive toward tension side of the beam).

In eqn. (2a), stresses were calculated from the measured strains using the following non-linear stress - strain relationship:

$$\sigma(\epsilon) = \sigma_o \cdot 10^{(1/e + 0.3)} \qquad (2b)$$

where

$e = \beta_0 + \beta_1 \cdot \xi + \beta_2 \cdot \xi^2 + \beta_3 \cdot \xi^3 + \beta_4 \cdot \xi^4 + \beta_5 \cdot \xi^5 + \beta_6 \cdot \xi^6$;
$\xi = \epsilon_o / \epsilon$;
$\epsilon_o = \sigma_o / E$;
σ_o = 0.2% offset yield stress; and
β_i = empirical coefficients fit to experimental uniaxial engineering stress - strain data.

The form of eqn. (2b) was selected to allow a closed-form fit to the experimental data.

Load Line Displacement Measurement

Load line displacement measurements were made using four eddy current displacement gages. These non-contacting transducers were placed under the SE(B) specimen as shown in Figure 2. The gages were offset from the load line

position to allow measurement of the bend angle imposed on the specimen using the following equation:

$$\theta = \mathrm{Tan}^{-1}\left[\frac{\Delta_2 - \Delta_1}{X}\right] + \mathrm{Tan}^{-1}\left[\frac{\Delta_3 - \Delta_4}{X}\right] \tag{3}$$

where
Δ_i = displacement at eddy current gage i; and
X = distance between centers of eddy current gage pair in numerator (51.6 mm).

This value of θ was used to calculate load line displacement as follows:

$$\Delta_{LL} = \frac{S}{2} \cdot \mathrm{Tan}\,(\theta/2) \tag{4}$$

This equation was derived by assuming rigid rotation of the specimen arms. By basing the load line displacement on differential displacement values (Δ_2-Δ_1 and Δ_3-Δ_4), the additional displacement due to elastic compression of the loading anvils is negated, because this component is equal in all four individual displacement measurements.

Crack Initiation Detection

During impact experiments, the conventional methods used for quasi-static experiments to determine the time at which crack blunting stops and crack growth begins are generally not applicable. Unloading compliance methods cannot be used, and the direct current potential drop (DCPD) technique, while useful for non-ferrous alloys, cannot be used for ferrous materials due to the magneto-elastic spike demonstrated by Hackett, et al. [12] which overwhelms the crack growth induced potential change. The alternating current potential drop (ACPD) technique shows promise [13], but suffers from analytical complexity. In this investigation, the utility of placing small strain gages in close proximity to the crack tip was investigated as a simple alternative that would be generically applicable to both ferrous and non-ferrous metals.

In developing a candidate procedure, it was desired to locate a position at which strain could be measured such that there would be an inflection point in a plot of load vs. strain indicative of crack initiation. To this end, the elastically loaded region behind the fatigue crack tip, illustrated schematically in Figure 3a, was examined. In this region, strains increase in proportion to the applied load, with the proportionality constant dependent on elastic modulus, gage orientation, and the specimen geometry. Crack initiation and growth changes the specimen geometry, which increases this proportionality constant. This concept is illustrated schematically in Figure 3b. In practice, the strain reversal shown in Figure 3b will probably not be as sharp owing to the gradual nature of the plastic crack tip blunting process. However, a reversal in the load vs. gage strain trace (or a deviation from linearity) should still be related to the onset of crack growth.

TENSILE TESTING

Tensile tests were conducted on the two steels at room temperature (+23°C) to determine the stress-strain behavior for the SE(B) specimen load analysis. Strains were measured on each specimen with two diametrically opposed high-elongation strain gages. These gages were shunt calibrated and conditioned through a high frequency amplifier having a maximum frequency response of 50 khz. Quasi-static tests were conducted in a screw driven tensile machine at a constant crosshead rate with load measured using a calibrated load cell. High rate tests were conducted in a drop tower using the special procedures described below.

Impact loading of the tensile specimens was achieved by placing them in a dynamic tensile rig, illustrated in Figure 4. This rig included a half-bridge strain gage load cell that was calibrated versus the load cell in a screw driven tensile machine. Following load calibration, the tensile rig was placed in the drop tower where the load was applied by a free-falling crosshead having a mass of 669 kg. The crosshead was dropped from 0.61 m to achieve an initial specimen displacement rate of 3.45 m/s. Two crossed

triangular wedges of soft aluminum were placed between the falling crosshead and the top of the tensile rig to allow a smooth load transfer between the falling crosshead and the rig. Load and strain signals were recorded on a four channel digital oscilloscope triggered by means of a fiber optic light beam broken by a flag attached to the falling crosshead.

RESULTS AND DISCUSSION

QUASI-STATIC EXPERIMENTS

One shallow crack SE(B) specimen of each material was tested at a quasi-static loading rate (ram speed < 0.01 mm/sec) so that control measurements of load and load line displacement could be made. Control load measurements were made using a calibrated load cell while control load line displacement measurements were made using a flex bar [14]. Comparisons between the load and load line displacement estimated using the candidate procedures and these control values are made in the following sections.

Load

Strains were measured at six equally spaced locations along the quarter span, as illustrated in Figure 1, so that load could be estimated by integrating the stress profile across the specimen width using eqn. (2). Numerical integration of this equation was achieved by partitioning the quarter span into a finite number of segments. While the number of segments used is arbitrary, insufficient discretization will bias the load estimate. To determine the number of segments needed to minimize this error, the load at 6 points during each test, as indicated on Figure 5, was estimated using various numbers of integration segments. The results of these calculations, shown in Figure 6, indicate that once the width of the specimen is partitioned into 40 or greater equal segments, the load estimated using eqn. (2) is no longer influenced significantly. For this reason, 40 integration segments were used in all subsequent load estimates made by numerically integrating

eqn. (2).

Figures 7 and 8 compare the control and strain gage load estimates for the two specimens tested. These data show that once a slight load is placed on the specimens (50 to 100 kN) the strain gage load estimate stays between 96% and 101% of the control load for the lower hardening material, and between 97% and 110% of the control load for the higher hardening material. While it would be preferable to have better agreement between the estimated and control loads for the higher hardening material, it will be demonstrated in a later section that this load error magnitude does not significantly effect the accuracy with which applied J can be calculated from these data. This indicates that this procedure for estimating the applied load from strain gage data has acceptable accuracy for load measurement during impact elastic-plastic fracture experiments.

Load Line Displacement

In Figures 9 and 10, the control load line displacement measured using the flex bar is compared to the load line displacement estimated by eqns. (3) and (4) using the four eddy current gages for the two specimens tested. These data indicate that the eddy current gage estimate of load line displacement considerably exceeds the control measurement, the error being most significant at small displacements. To investigate the cause of this discrepancy, a 3-D finite element model of the shallow crack SE(B) specimen was constructed using 324 20-node isoparametric elements, as shown in Figure 11. Symmetry of the loading and constraints permitted modeling of only one-quarter of the specimen. Elements incident on the crack front were degenerated into triangular prisms with the coincident nodes free to displace independently. This modeling procedure provides a 1/r strain singularity at all points along the crack front corresponding to element corner nodes. Reduced integration was used for all elements. Plasticity was modeled using incremental theory with a von Mises yield surface, an associated flow rule, and isotropic hardening. The material was assumed to have a bilinear uniaxial stress-strain curve having a slope of 206,850 MPa before yield, a slope of 6,895 MPa after

yield, and a yield stress of 675.7 MPa. Conventional, linear strain-displacement relations were employed by the computations. The finite element models were loaded by enforcing uniform vertical displacement of the nodes along a line at the top of the uncracked ligament and applying a load to the center point of this line. These computations were performed using POLO-FINITE software [15].

Figure 12 shows the deformed shape at the mid-thickness of the specimen's cracked side at various load levels as determined from this finite element model. These data indicate that the cracked side of the bar deforms into a curve, rather than as a straight line. This curved deformation causes eqns. (3) and (4) to overestimate load line displacement because the curved profile of the specimen is more displaced from the zero position than the straight line deformation assumed in deriving eqn. (3). To improve the accuracy of the load line displacement estimated by eqns. (3) and (4), eqn. (3) could be corrected for the error caused by the curved deformation, provided the magnitude of the error at each gage is easily calculable based on experimental measurements. Figure 13 shows that the deformed shape of the specimen predicted by the finite element analysis can be reasonably approximated by the cubic curvature of a beam elastically loaded in three point bending. This suggests that better agreement with the control values of load line displacement could be achieved by modifying eqn. (3) as follows:

$$\theta^* = \mathrm{Tan}^{-1}\left[\frac{\Delta_2 - \alpha\Delta_2^e - (\Delta_1 - \alpha\Delta_1^e)}{X}\right] + \mathrm{Tan}^{-1}\left[\frac{\Delta_3 - \alpha\Delta_3^e - (\Delta_4 - \alpha\Delta_4^e)}{X}\right] \quad (5)$$

where

α = empirical factor

Δ_i^e = elastic displacement at eddy current gage i calculated using the following equation:

$$\Delta_i^e = \frac{P}{48 \cdot EI}(3S^2x - 4x^3)$$

in this equation, x is the distance from the nearest roller support to the center of the eddy current gage. Thus, for gages 1 and 4, x = 22.1 mm, while for gages 2 and 3, x = 73.66 mm.

and using θ^* rather than θ in eqn. (4) to estimate load line displacement. Figures 14 and 15 show that load line displacement estimated using θ^* is in considerably better agreement with the control measurements (within ± 6% for both steels) than load line displacement estimated using θ. In these figures, the α value was selected to force the initial slope of load vs. load line displacement to match that expected for the initial precrack depth calculated using the elastic compliance equations presented in [16]. This makes the choice of α non-arbitrary, and further allows it to be made without the need for a control load line displacement to match, which is the case at impact loading rates. These data indicate that estimates of load line displacement made using this procedure have acceptable accuracy for load measurement during impact elastic-plastic fracture experiments.

J Calculation

In the preceding sections, it was demonstrated that both load and load line displacement can be determined using the candidate procedures to acceptable levels of accuracy for two materials of considerably different strain hardening capacity. Since the result of a fracture toughness test is an estimate of the fracture initiation toughness, it is of interest to determine how load and load line displacement estimation errors affect the accuracy with which J can be calculated using eqn. (1). Figures 16 and 17 compare the J values calculated using the control load and load line displacement data to J values calculated from load and load line displacement estimated using the candidate procedures discussed above. These data demonstrate that J values can be determined to within ± 3% of the control values using the candidate load and load line displacement estimation procedures once globally elastic load levels have been exceeded. This indicates that these procedures have acceptable accuracy for estimation of applied J values during impact elastic-plastic fracture experiments.

IMPACT EXPERIMENTS

A shallow crack SE(B) specimen of the lower hardening steel was tested in

a drop tower at an initial impact velocity of 4.88 m/s to a total displacement of 4.3 mm at which point the falling head was arrested on rigid stops, allowing the specimen to unload. Post test examination of the fracture surface indicated that this amount of deformation resulted in 2.1 mm of ductile crack growth at the specimen midplane. Figure 18 shows the load and load line displacement variation with time for this experiment; these values were estimated from the strain and displacement gage data as discussed previously. Figure 19 shows the load vs. load line displacement curve calculated using an α value of 0.60 in eqn. (5) to bring the initial load vs. load line displacement slope into agreement with that expected based on the initial precrack length.

The data presented in Figure 18 demonstrate that these strain and displacement measurements resolved load and load line displacement variations at microsecond intervals with sufficient response for impact fracture experiments where the maximum load plateau is reached 3 ms after initial load application. However, because eqn. (1) considers only the effects of deformation energy (ω) and not of kinetic energy (K) in the calculation of J, the error introduced by this simplifying assumption needs to be determined before these load and load line displacement values can be used with confidence to calculate an initiation fracture toughness value. Nakamura, et al. [17] developed a model from which the ratio of kinetic energy to deformation energy (K/ω) can be calculated as a function of time based on load line displacement measurements. This model is as follows:

$$\frac{K}{\omega} = \left[\left(\frac{S \cdot B \cdot E \cdot C_s}{2 \cdot W} \right)^{1/2} \cdot \frac{W}{c_o} \cdot \frac{\dot{\Delta}_{LL}(t)}{\Delta_{LL}(t)} \right]^2 \qquad (6)$$

where

C_s = elastic compliance
c_o = longitudinal bar wave speed

Nakamura et al. [17] demonstrated that eqn. (6) provides good estimates of the K/ω ratio for a SE(B) specimen with an a/W of 0.5 by comparing the predictions

of eqn. (6) to K/ω values determined directly from a dynamic finite element model of the SE(B) specimen. Therefore, eqn. (6) was used for to analysis of data from the shallow cracked SE(B) ($a/W \approx 0.1$) of this study because the assumptions made in the derivation of eqn. (6) (the presence of the crack was ignored and it was assumed that plastic deformation is insignificant when K/ω exceeded unity) were better satisfied by the shallow crack case. Figure 20 shows the variation of K/ω with time for the impact loaded SE(B) specimen. These data indicate that the K/ω ratio was quite small (less than 0.1) after 1.75 ms elapsed. At this time, the specimen was still subjected to globally elastic loading (load < 100 kN) and crack initiation had not yet occurred. This demonstrates that ignoring the effects of kinetic energy in calculating the crack initiation toughness of a shallow crack SE(B) loaded at impact rates does not significantly influence the J_i estimate because the amount of kinetic energy in the specimen is small compared to the amount of deformation energy from very early in the loading history.

CRACK INITIATION DETECTION

To test the candidate procedure for detecting crack initiation previously described, a shallow crack SE(B) specimen of the lower hardening steel was instrumented with two foil strain gages bonded close to the crack tip (Figure 3) in addition to the load and load line displacement instrumentation. Gages of two different grid sizes were attached at the same nominal position and orientation (2.54 mm behind the crack tip, 3.56 mm above the crack line, perpendicular to the crack line) with respect to the crack tip. The specimen was allowed to displace 4.85 mm at the load line before the falling cross-head was arrested onto rigid stops, a displacement which resulted in 4.70 mm of crack growth at the specimen mid-plane. Figure 21 shows the resulting load vs. load line displacement and load vs. crack tip strain traces. Only the strain measured by smaller gage (gage length of 0.79 mm, grid area of 0.64 sq-mm) showed a strain reversal with increasing load, while the larger gage (gage length of 1.57 mm, grid area of 2.46 sq-mm) measured larger strains that increased continuously with increasing load. It was reasoned that both gages had been placed too close to the elastic-plastic boundary, and that a better

defined strain reversal could be achieved by moving the gages further into the elastic region. The selected gage position was 3.56 mm behind the crack tip and 2.54 mm above the crack line; this position precluded use of the large strain gage. A specimen so instrumented was impact tested and allowed to displace 3.33 mm at the load line, resulting in 1.52 mm of crack growth at the specimen mid-plane. Figure 22 shows the load vs. load line displacement and load vs. crack tip strain traces in which definite clear reversals of strain with load were observed. Several more impact experiments were planned to be conducted at progressively lower levels of total load line displacement until no crack growth was observed. In practice, the arrestor mechanism on the drop tower could not be controlled to the degree needed to achieve these conditions.

As an alternative to further impact experiments, two quasi-static experiments were conducted to allow close control on the displacement at which the test was stopped. One test was halted after the load vs. strain reversal occurred, while the other was halted just as the reversal began. The data from these two experiments is presented in Figures 23 and 24, respectively. After the tests, the specimens were heat tinted and fractured at liquid nitrogen temperature (-195^{o}C). Neither specimen showed macroscopic evidence of crack initiation. However, a scanning electron microscope examination of the fracture surfaces revealed pockets of ductile growth between the fatigue crack and the final cleavage fracture on both specimens, as illustrated in Figure 25. These data suggest that the reversal in the load vs. crack tip strain plots of Figures 22 through 24 is closely associated with ductile crack initiation from the fatigue crack, making this strain measurement sensitive and useful for inferring the time at which crack initiation occurs. This information, combined with the load and load line displacement data, allows an initiation fracture toughness value to be calculated from the results of impact tests of shallow cracked SE(B) specimens. It should be noted, however, that the applicability of this method to different materials may depend upon both the strain hardening exponent and the initiation fracture toughness of the material being tested.

SUMMARY AND CONCLUSIONS

In this investigation, techniques useful for estimating load, load line displacement, and the time of crack initiation during impact tests of single edge notched bend, SE(B), specimens having shallow fatigue cracks ($a/W \approx 0.1$) were developed and validated. In particular, the following conclusions result:

1. The load applied to a shallow crack SE(B) specimen can be estimated by integrating the distribution of stress across the arm of the specimen midway between the loading and support points. Information regarding the variation of bending strain with position across the specimen arm and the uniaxial engineering stress-strain curve are needed to make this estimate. These estimates of load compared favorably with control measurements made during quasi-static SE(B) tests of two alloy steels, one having low and one having high strain hardening characteristics.

2. The load line displacement experienced by a shallow cracked SE(B) specimen can be estimated from displacements measured at four locations on the cracked face of the specimen, two on each side of the crack. These measurements were used to calculate the bend angle experienced by each half of the specimen, the load line displacement was then estimated by assuming rigid rotation. Once corrected for the non-linear deformation of the specimen using a simple formula derived from Euler beam theory, these estimates compared favorably with control measurements made during quasi-static SE(B) tests of two alloy steels, one having low and one having high strain hardening characteristics.

3. It is appropriate to ignore the effects of kinetic energy when calculating an initiation fracture toughness value from load and load line displacement data for shallow cracked SE(B) specimens loaded at up to 4.88 m/s because this energy is a small fraction of the deformation energy in the specimen at the time of crack initiation. This finding was demonstrated by dynamic testing of a low hardening alloy steel.

4. The occurrence of a strain reversal in a plot of applied load vs. strain normal to the crack plane measured in the elastically loaded region behind the crack tip in a shallow cracked SE(B) specimen served as a sensitive indicator of crack initiation from the fatigue crack. This finding was demonstrated by quasi-static and dynamic testing of a low hardening alloy steel.

Table 1: Tensile Properties of the Steels Investigated

Material	Loading Rate [mm/s]	0.2% Offset Yield Strength [MPa]	Ultimate Tensile Strength [MPa]	Reduction in Area [%]	Elongation over 25.4 mm Gage Length [%]
Low Hardening (HY-100)	0.01	745	841	66	--
		800	889	63	27
		793	883	62	29
	3454	827	986	61	31
		820	986	63	34
		841	---	61	30
High Hardening (ASTM A515 Gr. 70)	0.01	287	543	52	34
		314	547	51	36
		297	536	51	32

Tensile properties measured using a round bar specimen having an initial diameter of 7.95 mm and an initial gage length of 25.4 mm.

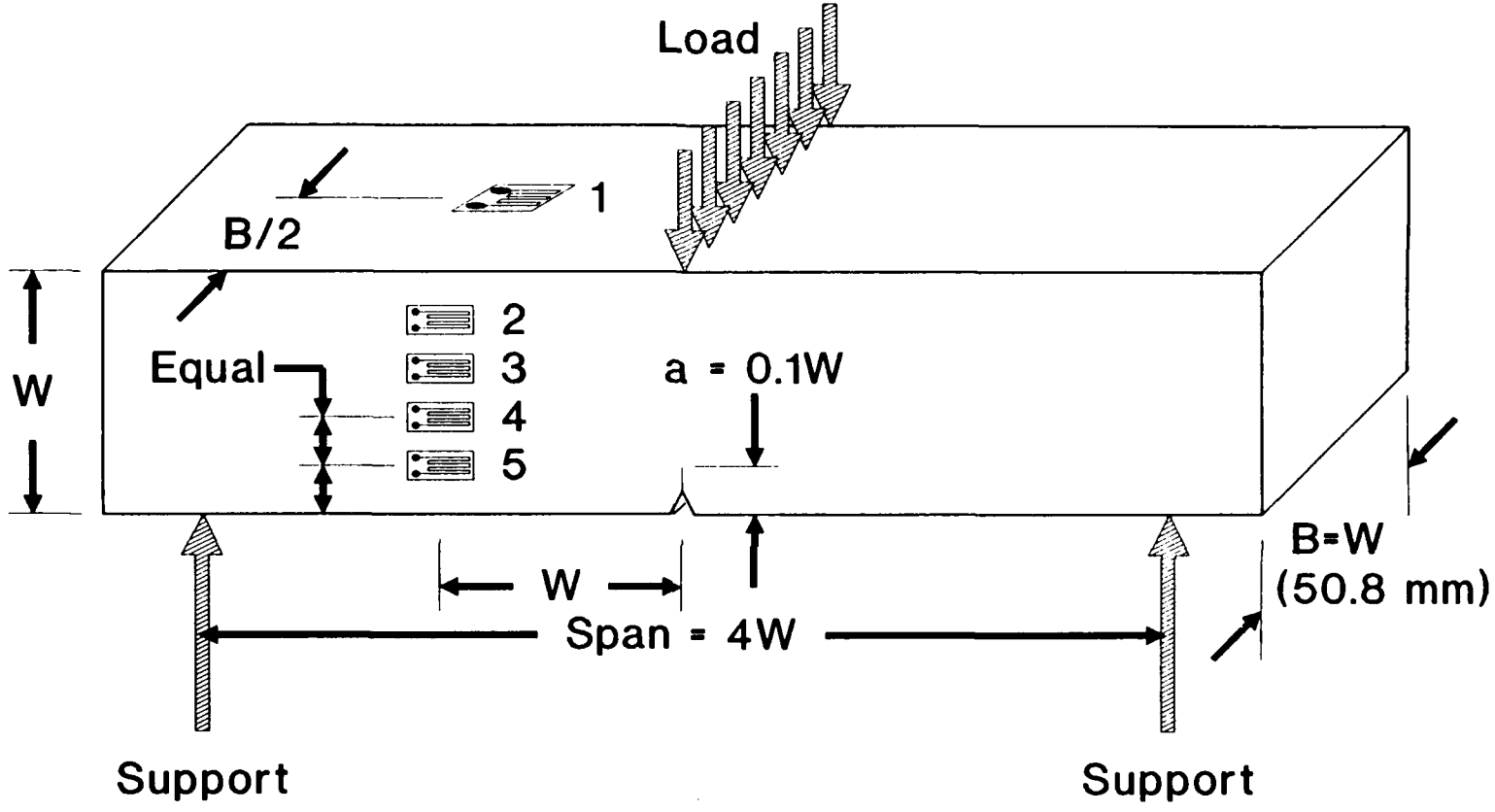

Note: Gage 6 is located on the cracked face in the same position as Gage 1.

Figure 1: Diagram of shallow crack SE(B) specimen showing position of quarter span strain gages used to estimate load.

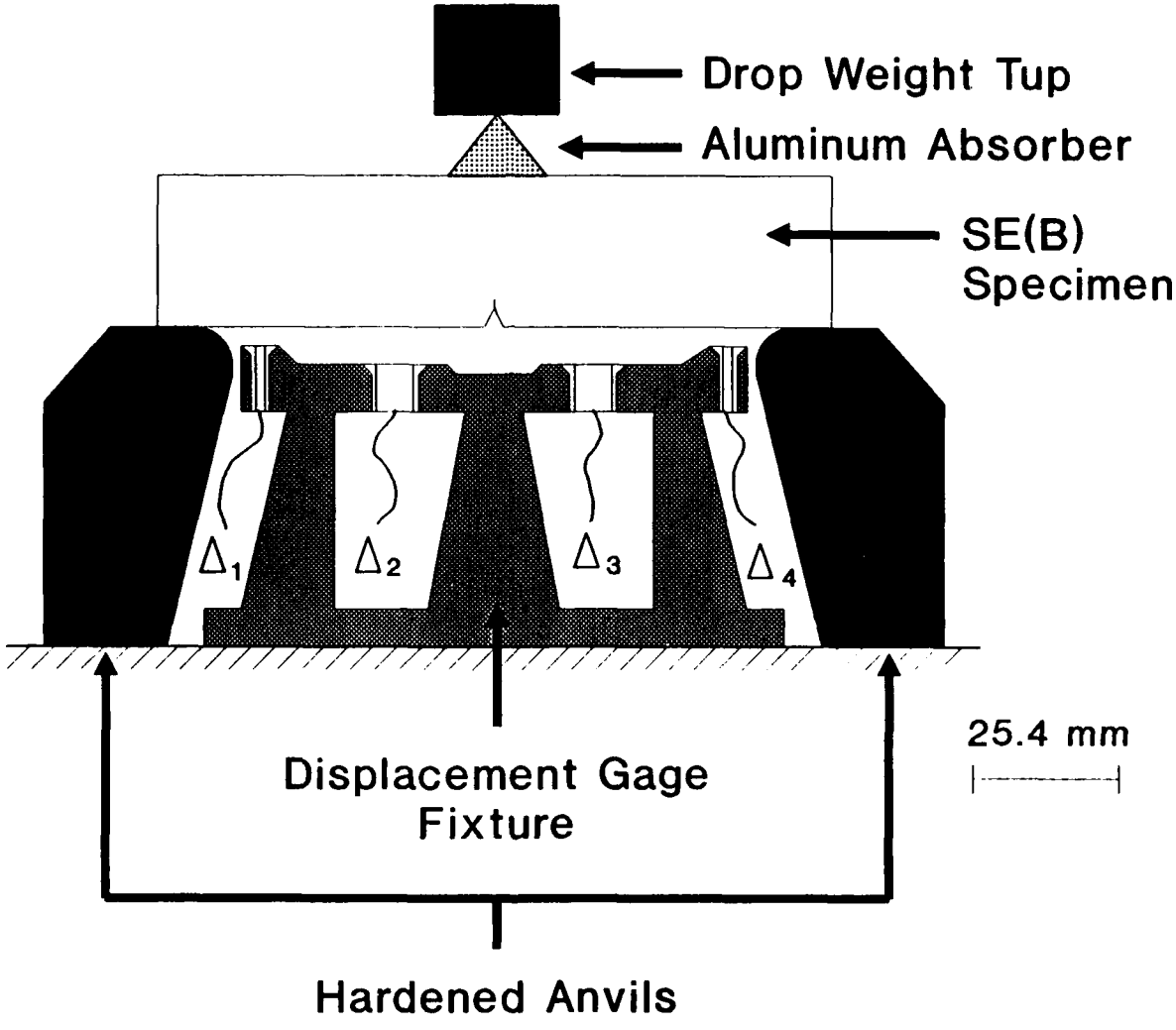

Figure 2: Diagram of non-contacting eddy current displacement gages (Δ_1, Δ_2, Δ_3, and Δ_4) positioned in the apparatus used to conduct SE(B) experiments.

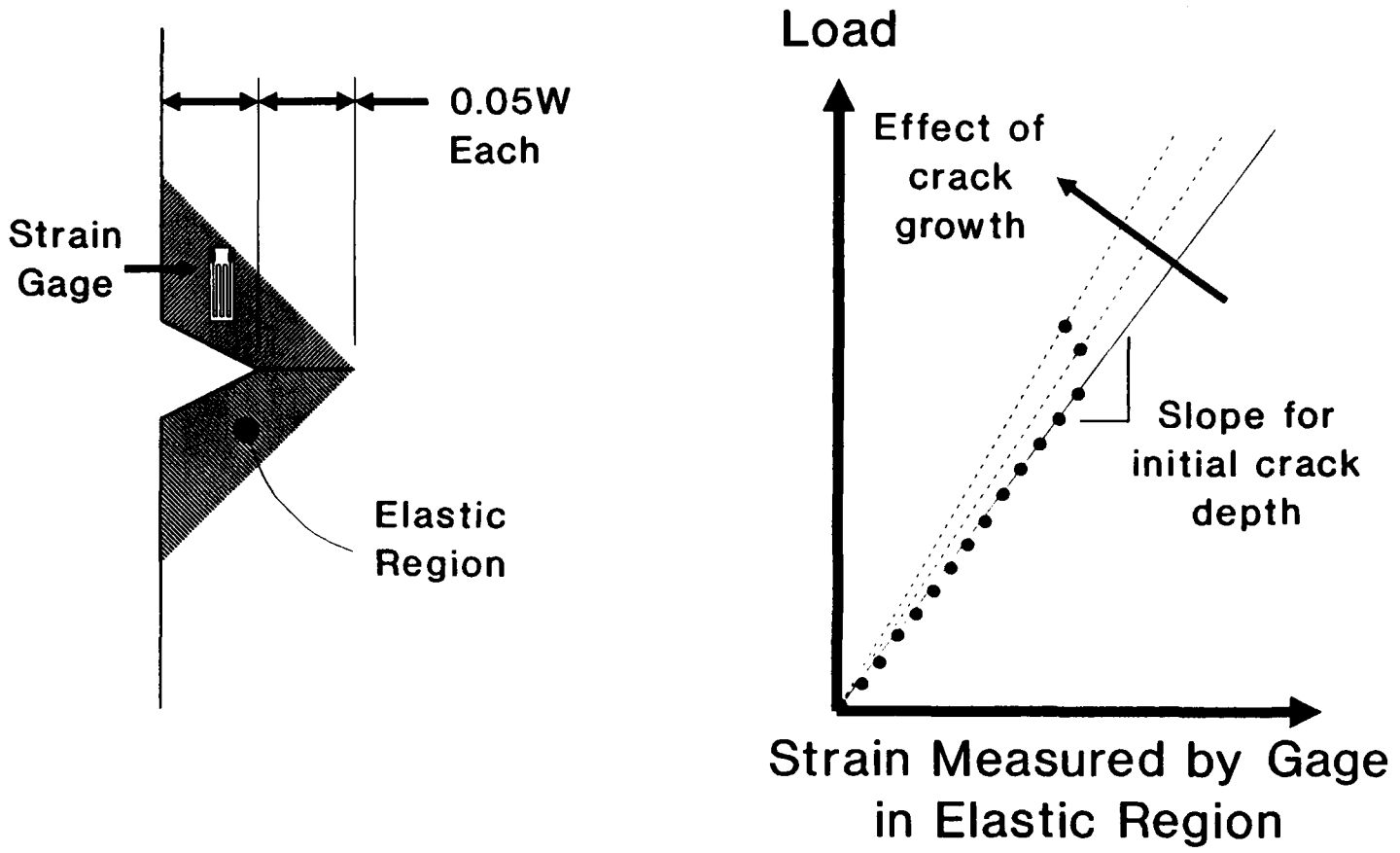

Figure 3: (a) Specimen region for strain measurement to infer crack initiation during shallow crack SE(B) experiments, and (b) anticipated load - strain response of a gage located in this region.

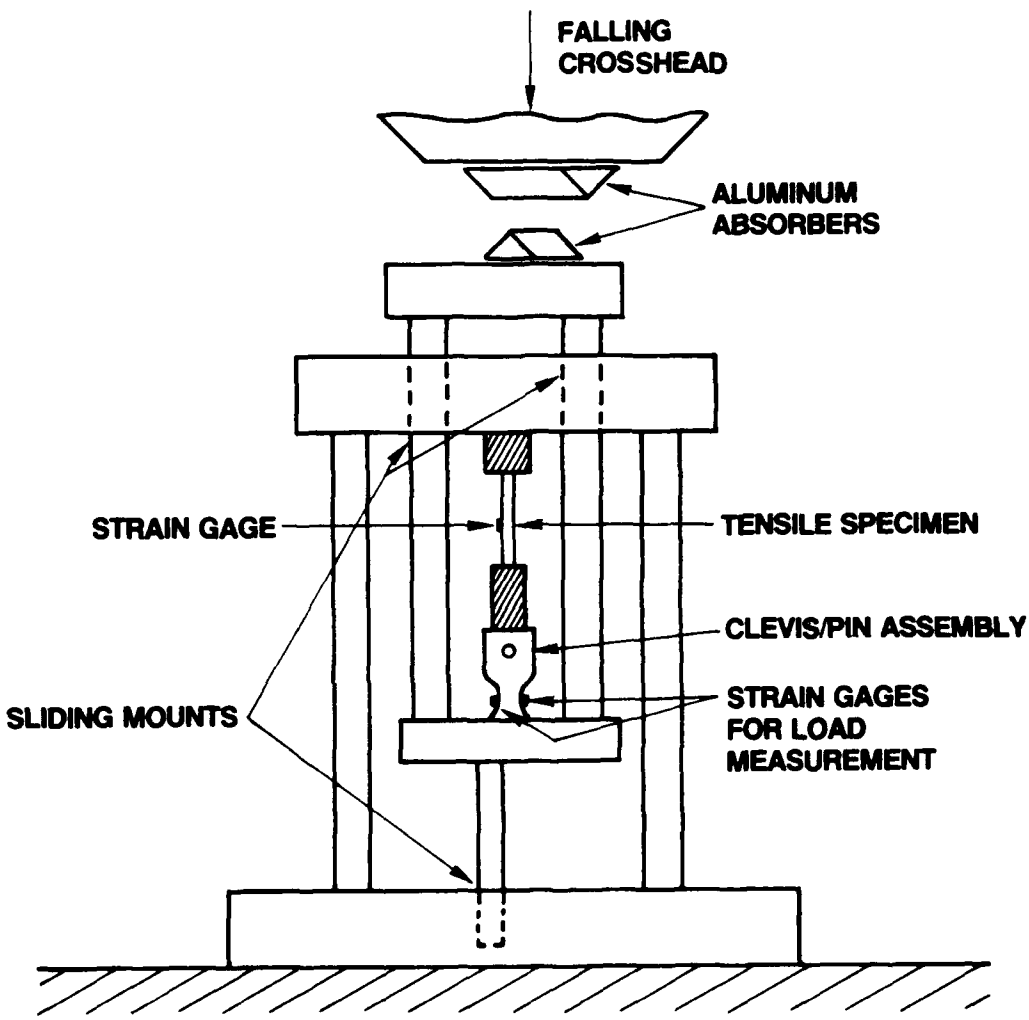

Figure 4: Apparatus used to conduct dynamic tensile tests.

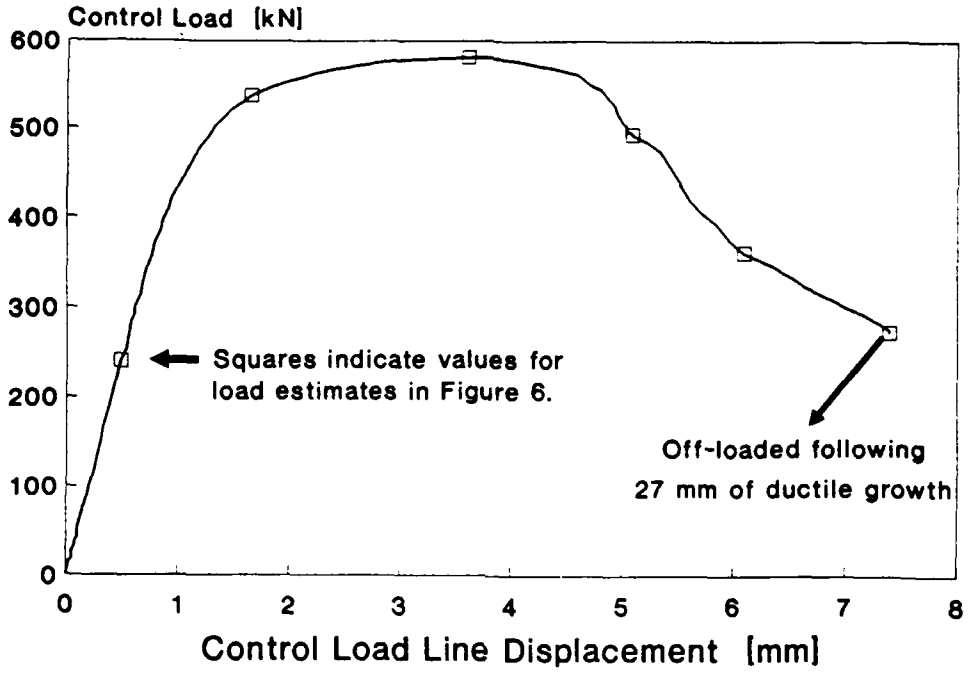

(a)

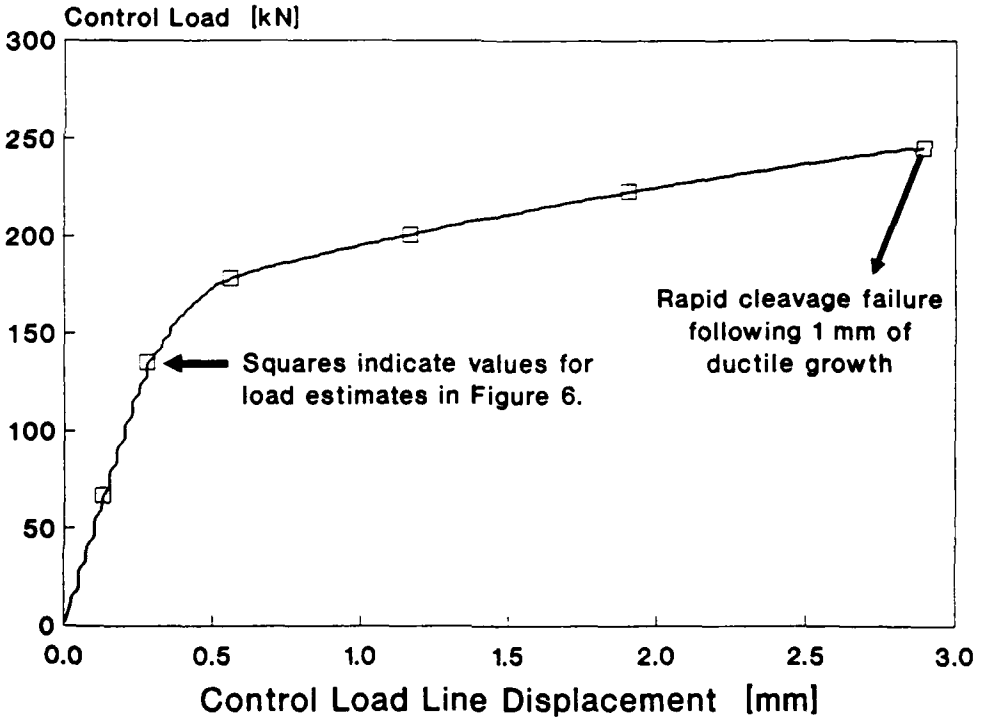

(b)

Figure 5: Control records of load vs. load line displacement recorded during quasi-static shallow cracked SE(B) tests of an (a) low, and a (b) high hardening steel alloy.

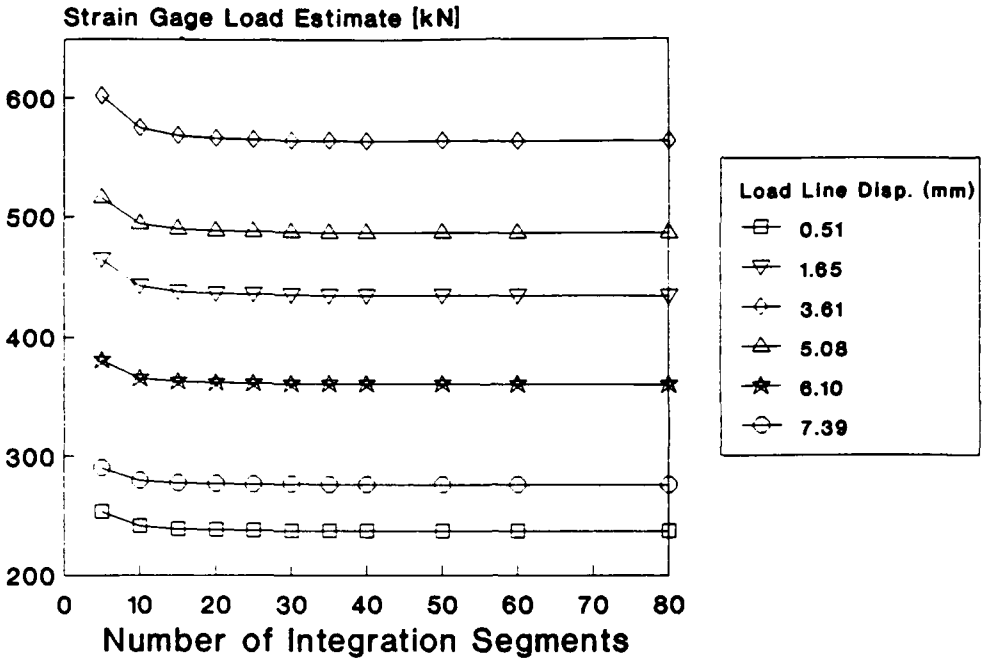

(a)

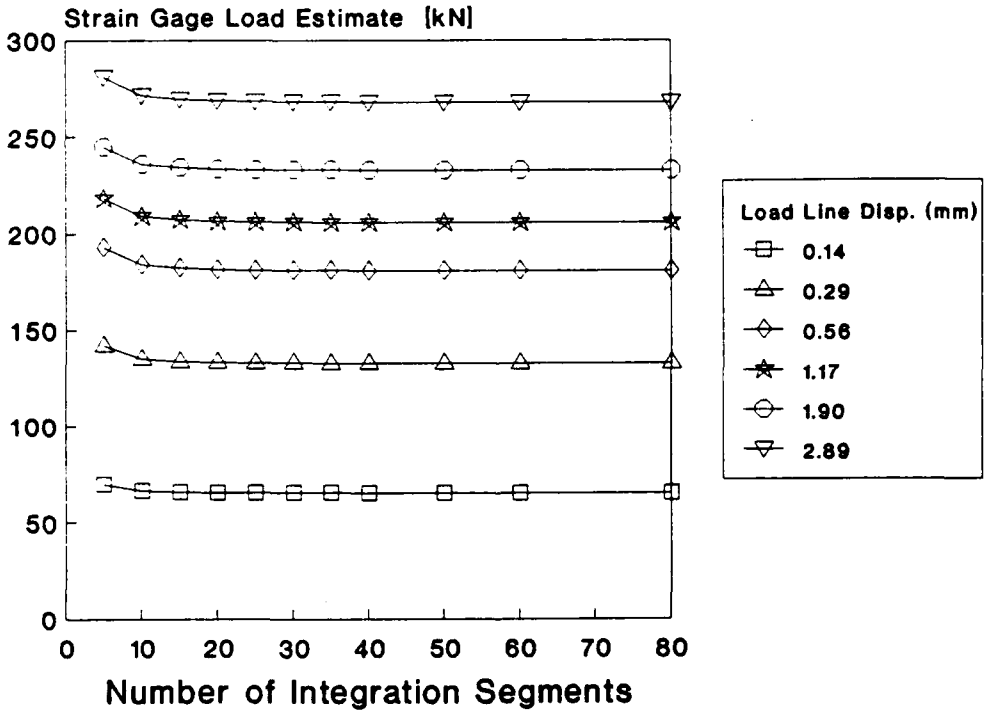

(b)

Figure 6: Effect of number of integration segments on load estimated from strain gage measurements using eqn. (2a) for the (a) low and for the (b) high hardening steel.

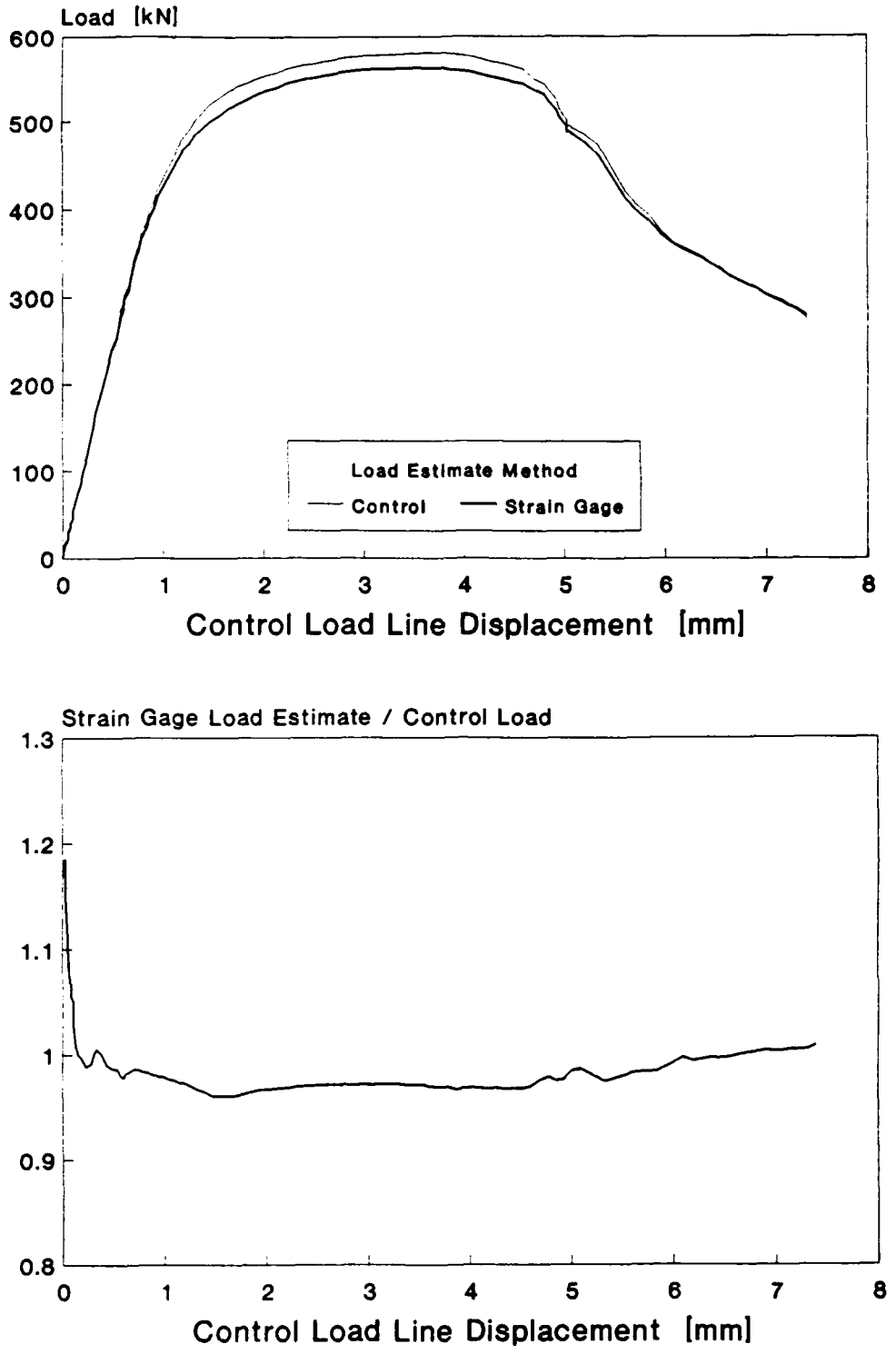

Figure 7: A comparison between the load estimated from strain gage measurements using eqn. (2a) and the control load for the low hardening steel.

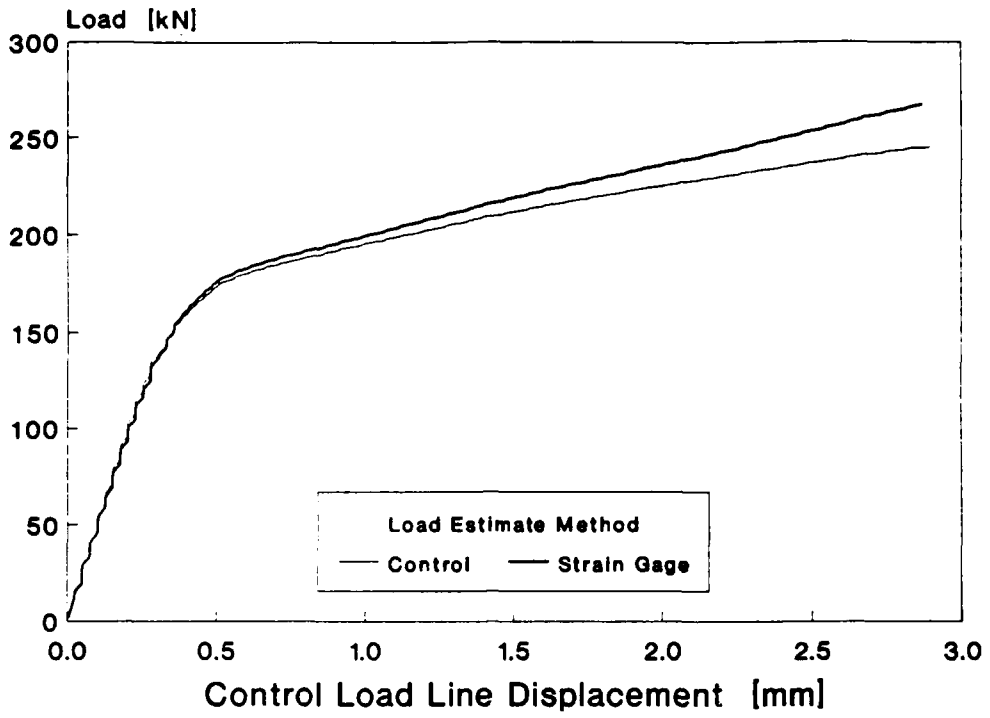

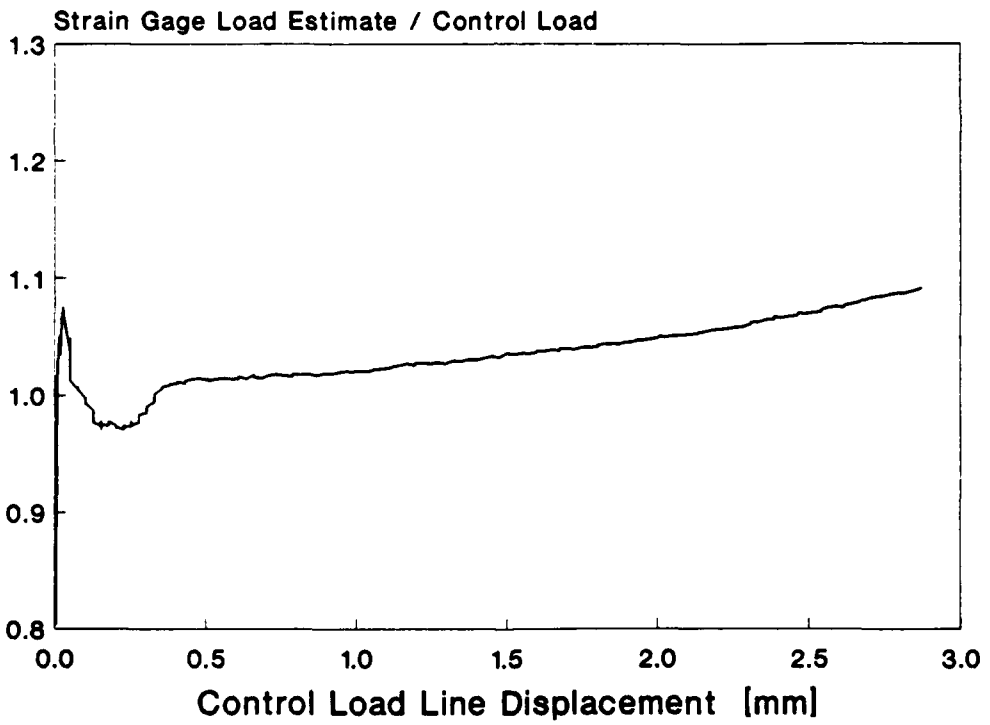

Figure 8: A comparison between the load estimated from strain gage measurements using eqn. (2a) and the control load for the high hardening steel.

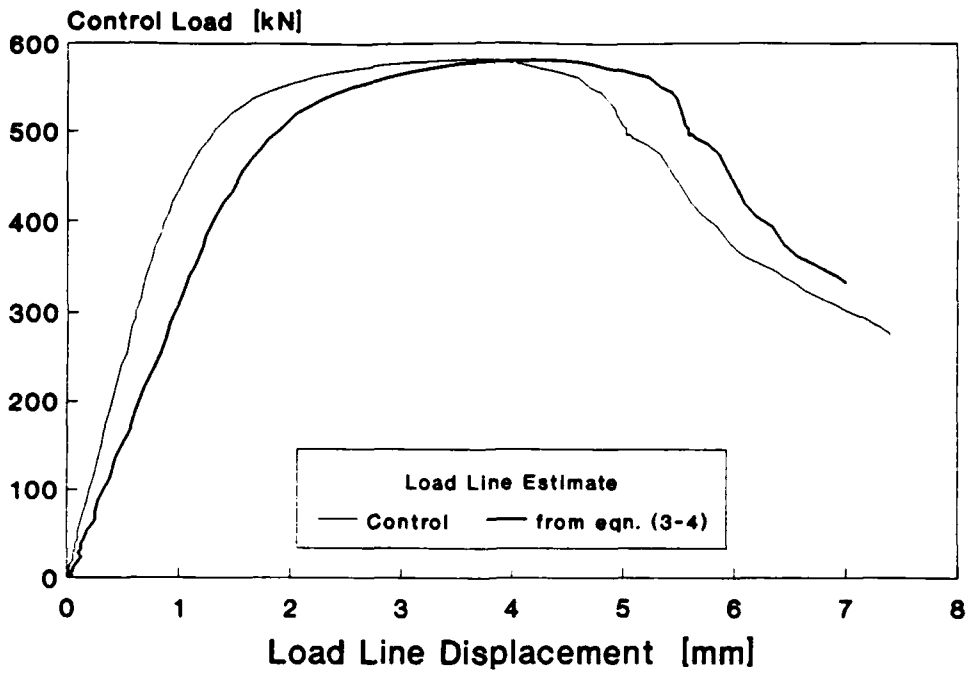

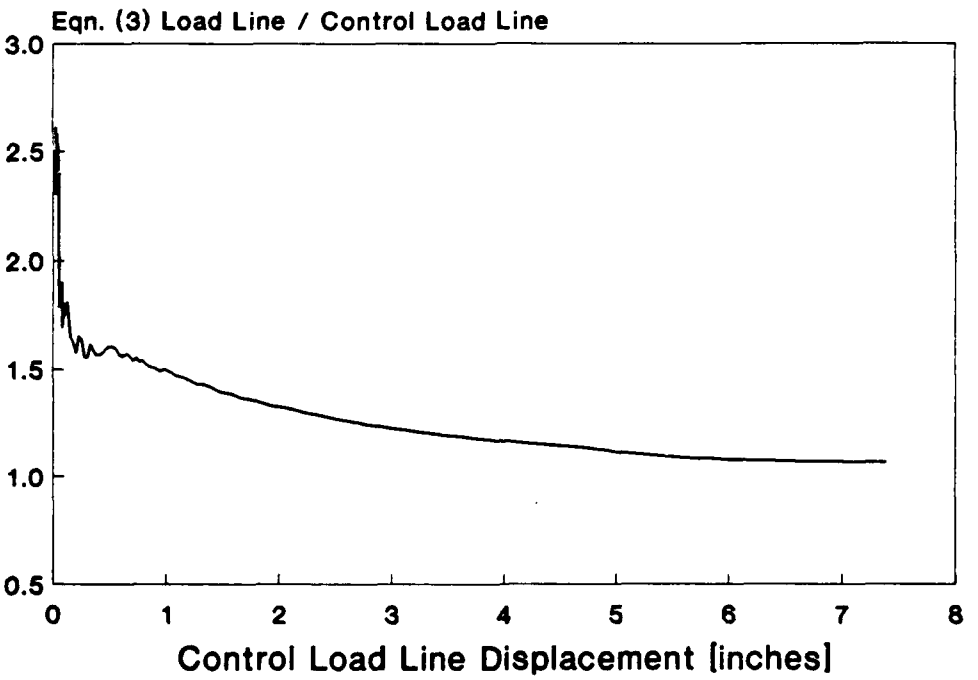

Figure 9: A comparison between the load line displacement estimated from the eddy current displacement measurements using eqns. (3-4) and the control load line displacement for the low hardening steel.

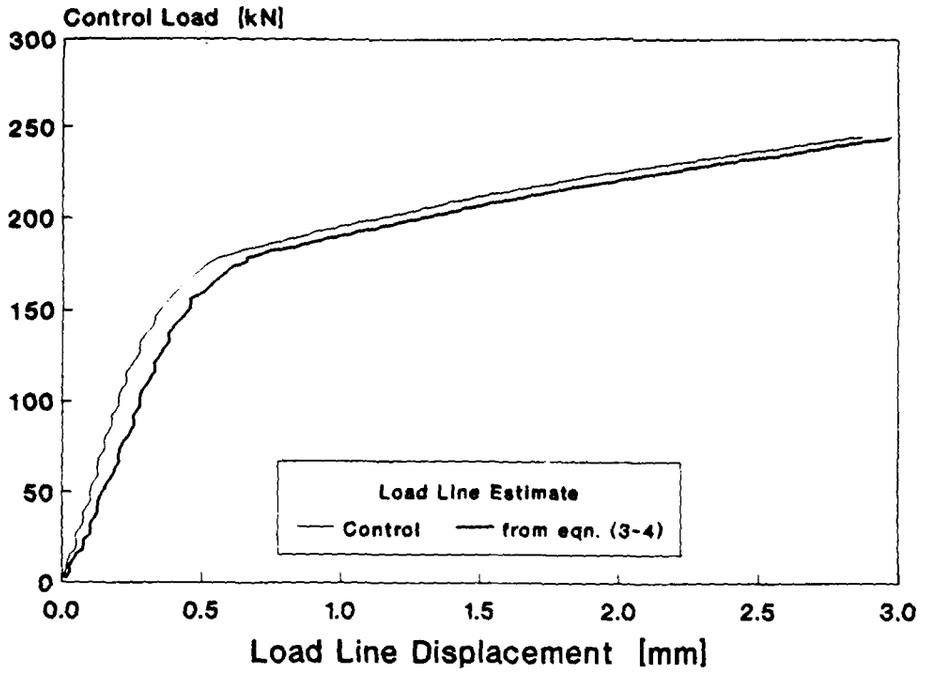

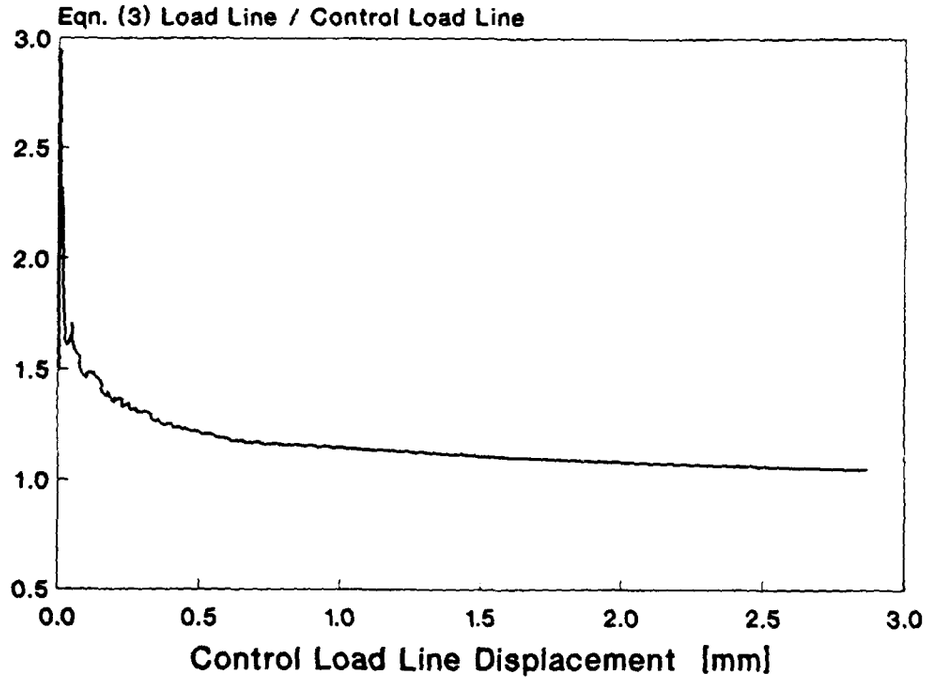

Figure 10: A comparison between the load line displacement estimated from the eddy current displacement measurements using eqns. (3-4) and the control load line displacement for the high hardening steel.

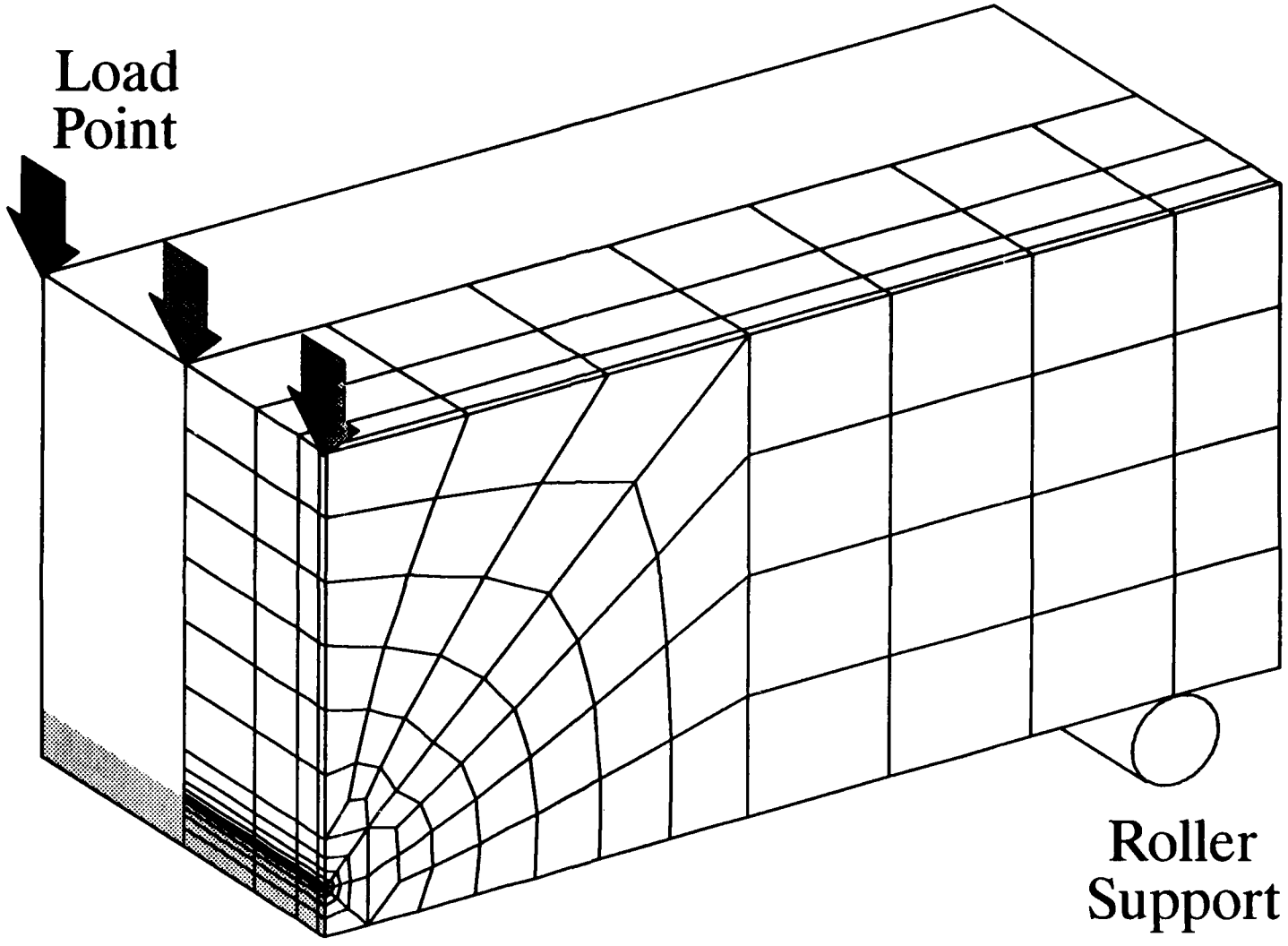

Figure 11: Finite element model of the shallow crack SE(B) specimen.

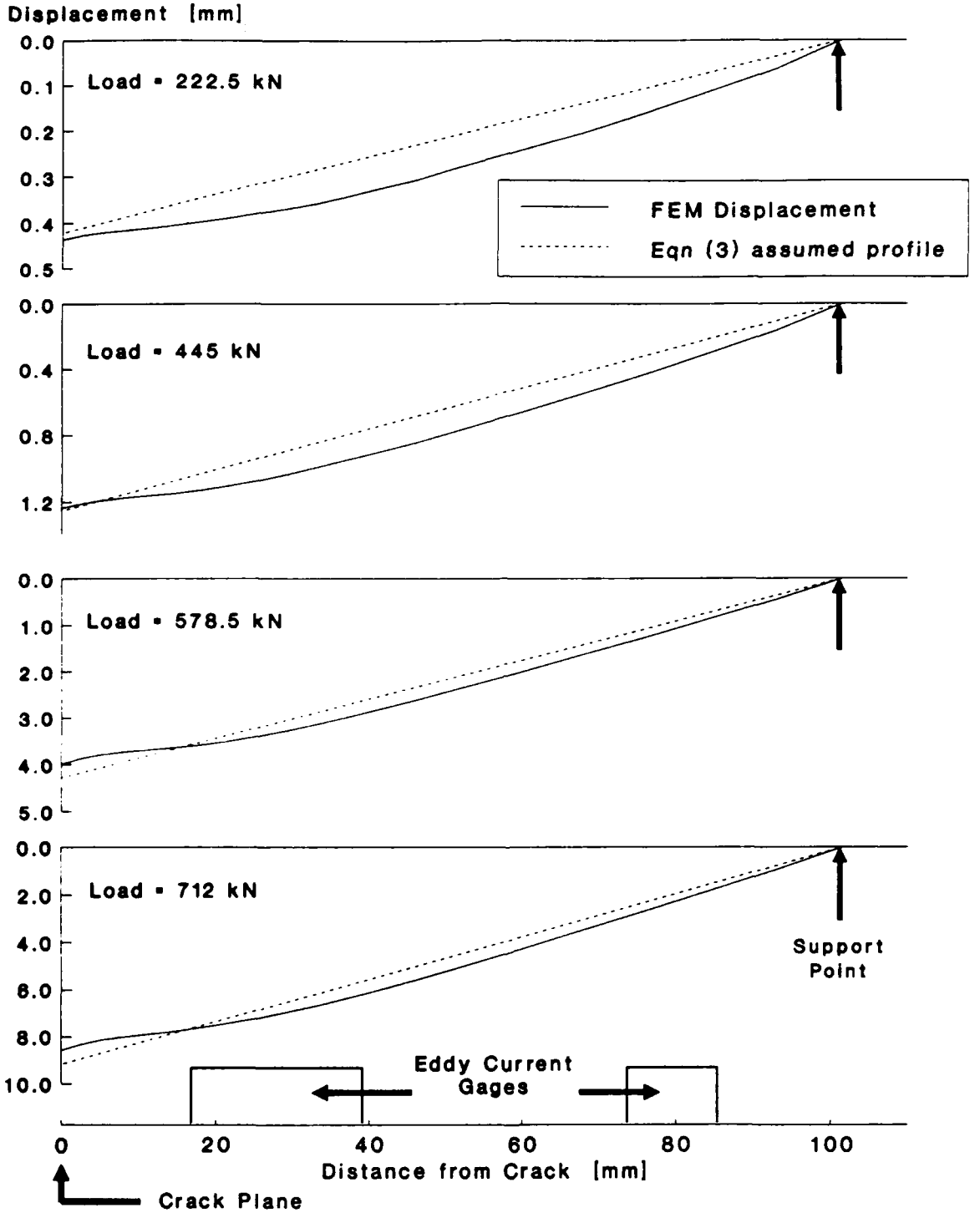

Figure 12: Comparison of the displaced profile at the mid-thickness of the cracked side of the SE(B) specimen predicted using finite elements and that assumed in the derivation of eqn. (3) at various load levels.

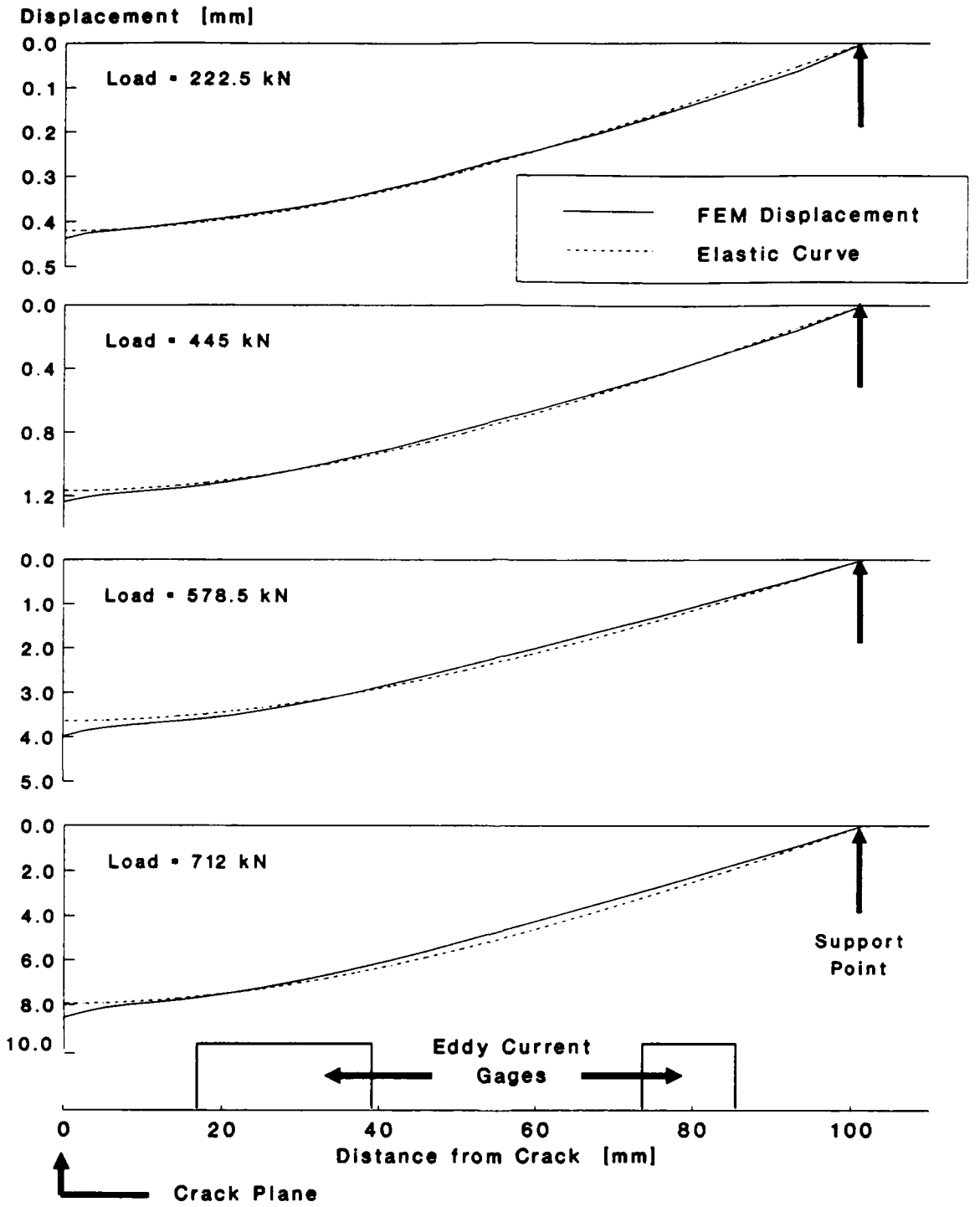

Figure 13: Comparison of the displaced shape at the mid-thickness of the cracked side of the SE(B) specimen predicted using finite elements and that of a beam elastically loaded in three point bending.

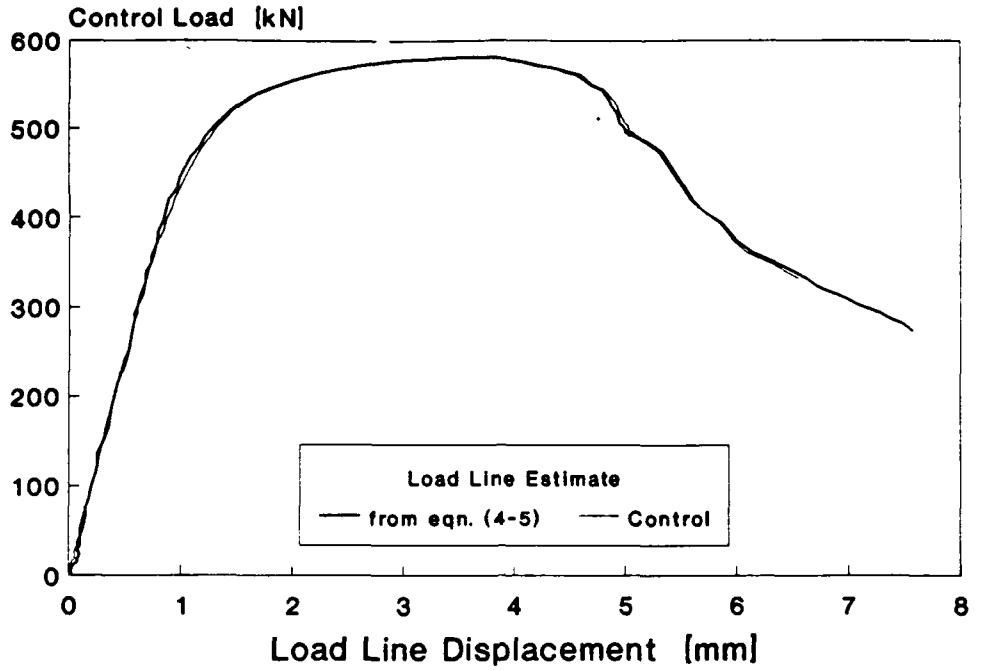

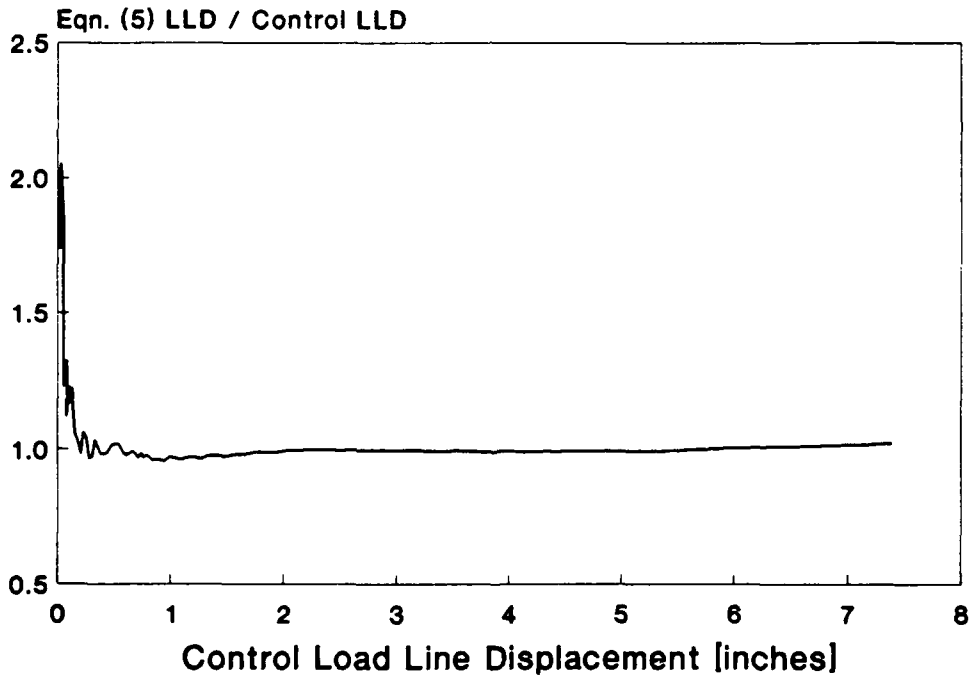

Figure 14: A comparison between the load line displacement estimated from the eddy current displacement measurements using eqns. (4-5) and the control load line displacement for the low hardening steel.

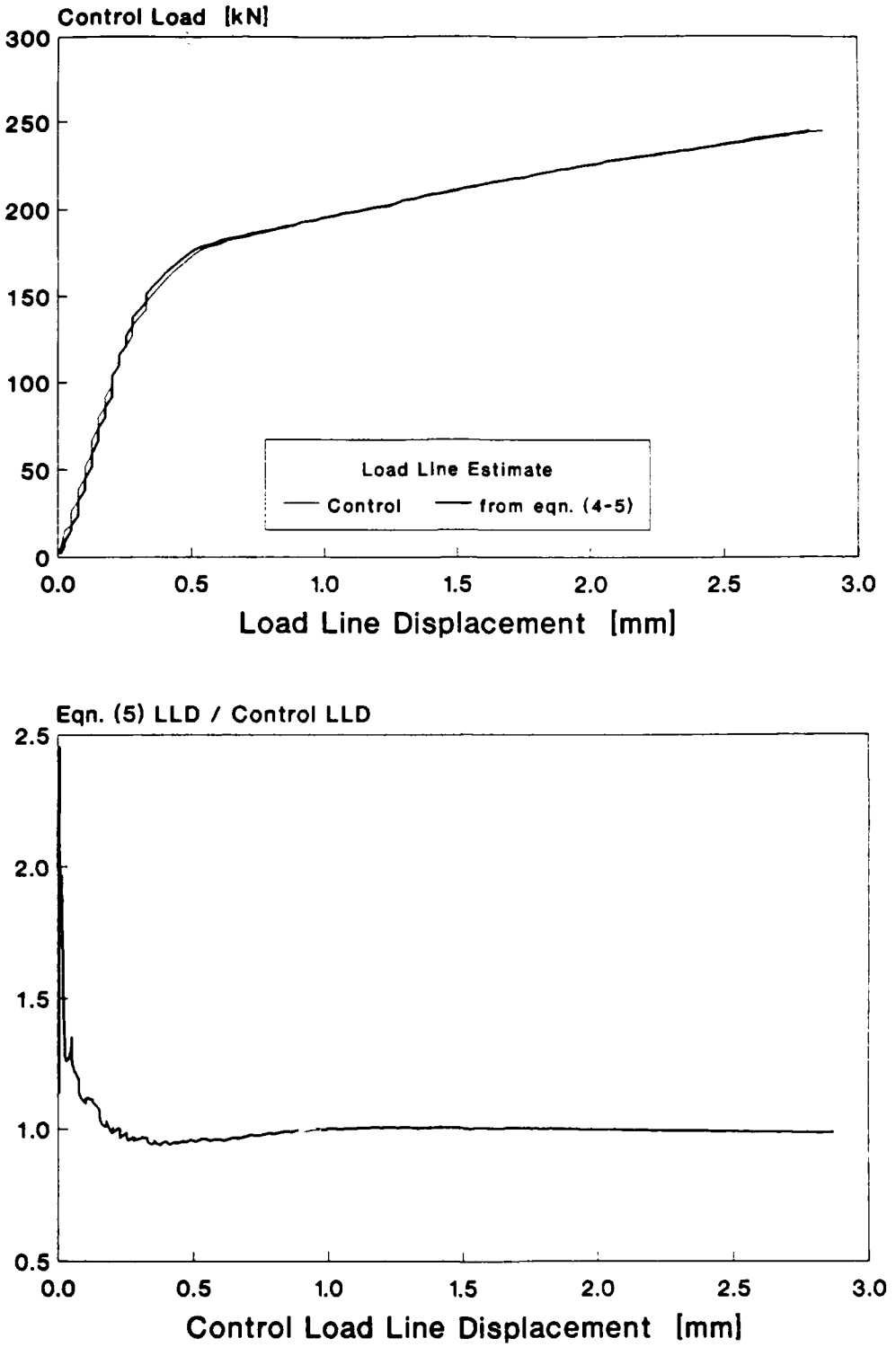

Figure 15: A comparison between the load line displacement estimated from the eddy current displacement measurements using eqns. (4-5) and the control load line displacement for the high hardening steel.

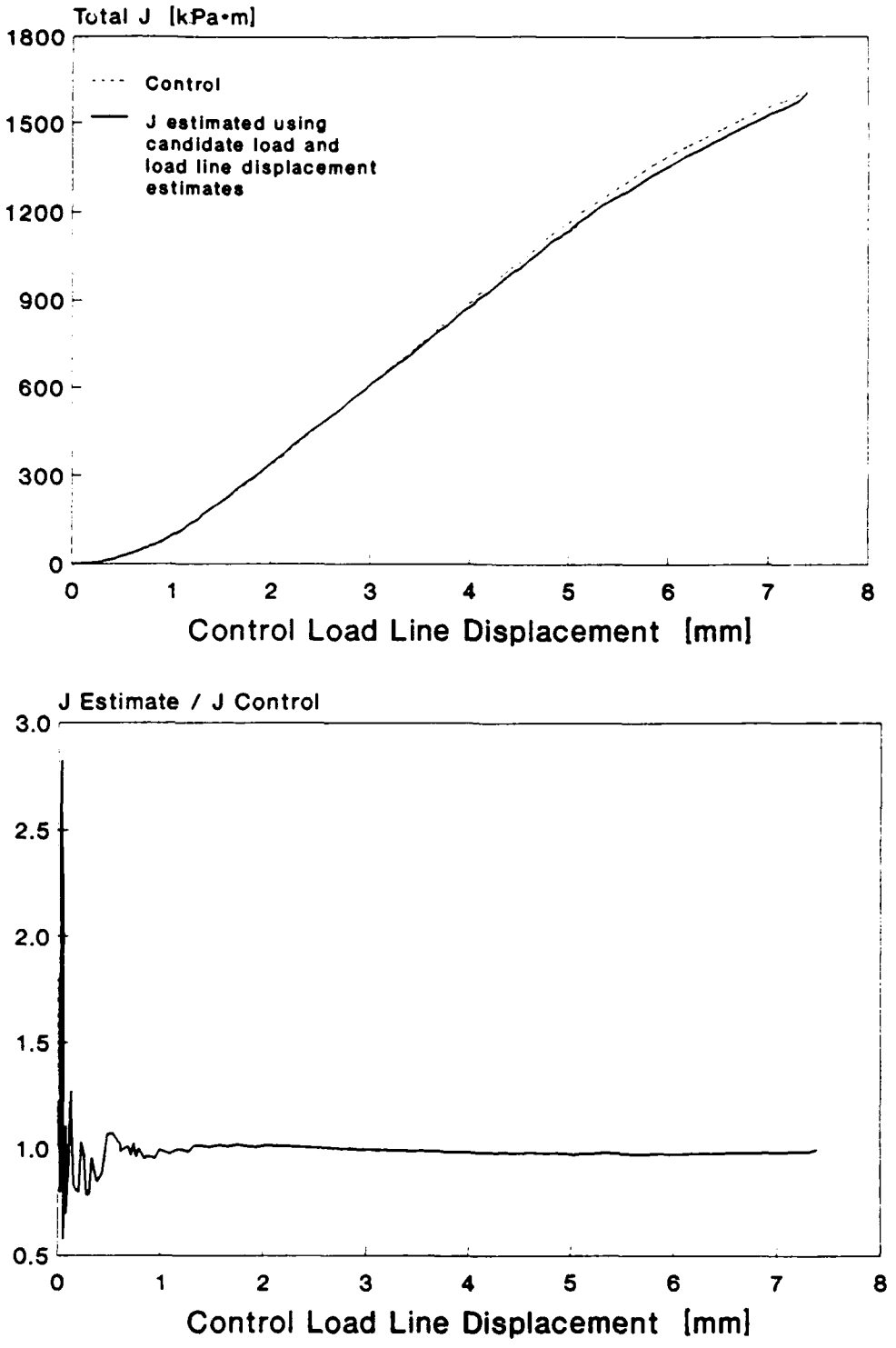

Figure 16: A comparison of applied J calculated from the reference load and load line displacement estimates with that calculated from load and load line displacement estimated using the candidate procedures for the low hardening steel.

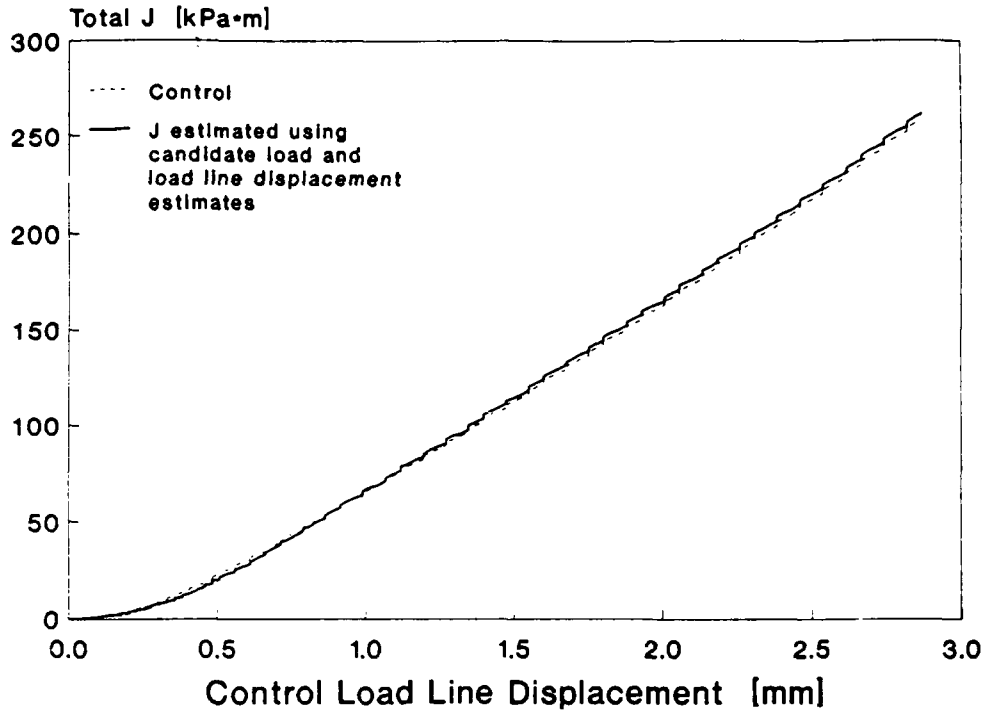

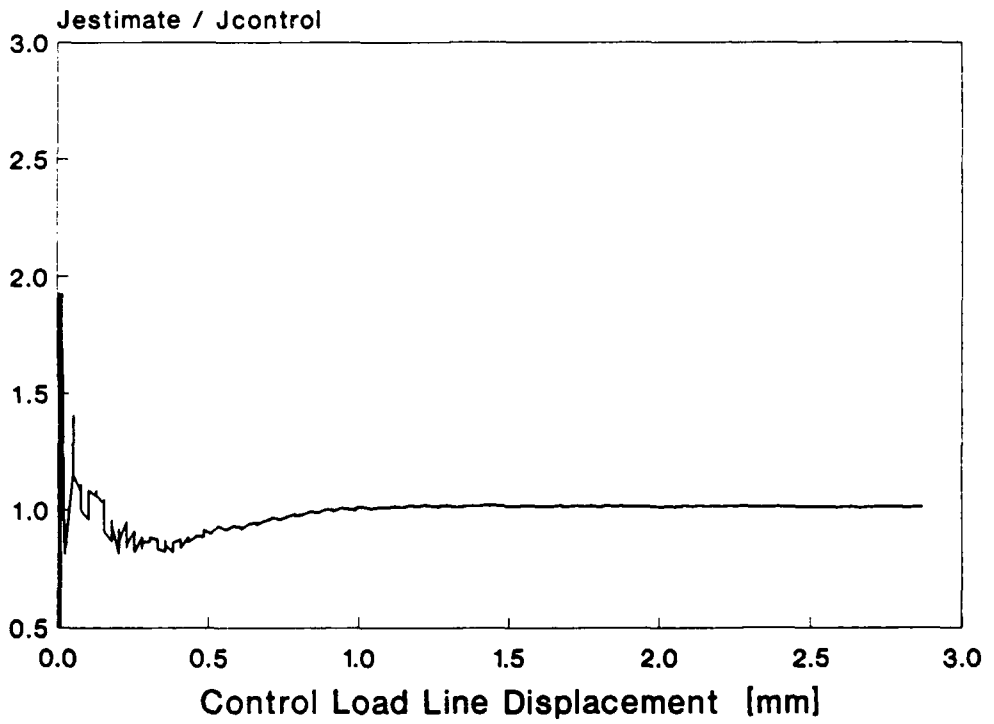

Figure 17: A comparison of applied J calculated from the reference load and load line displacement estimates with that calculated from load and load line displacement estimated using the candidate procedures for the high hardening steel.

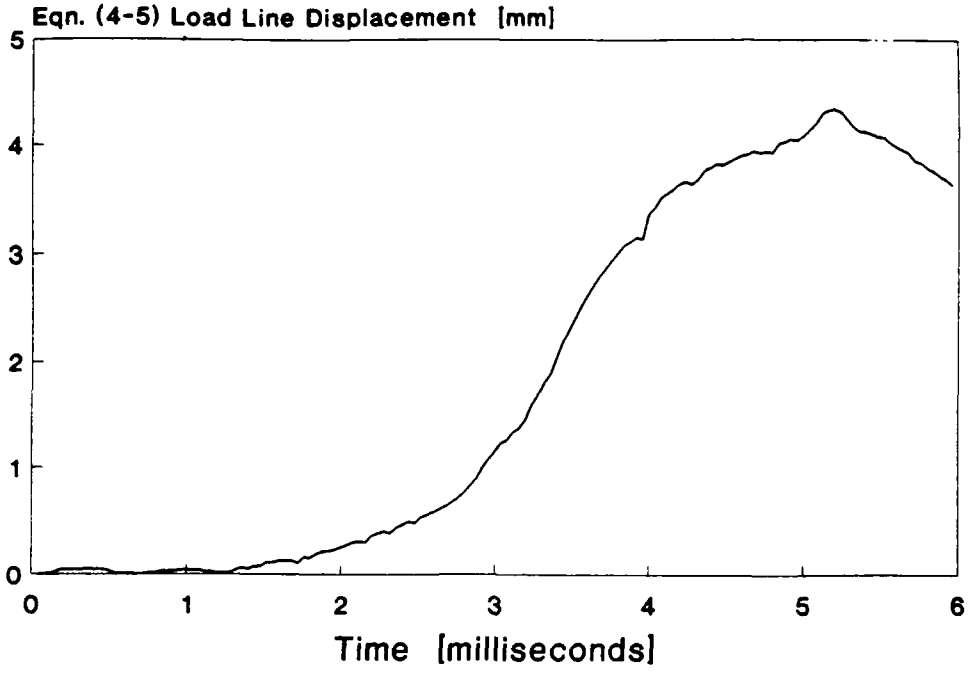

(a)

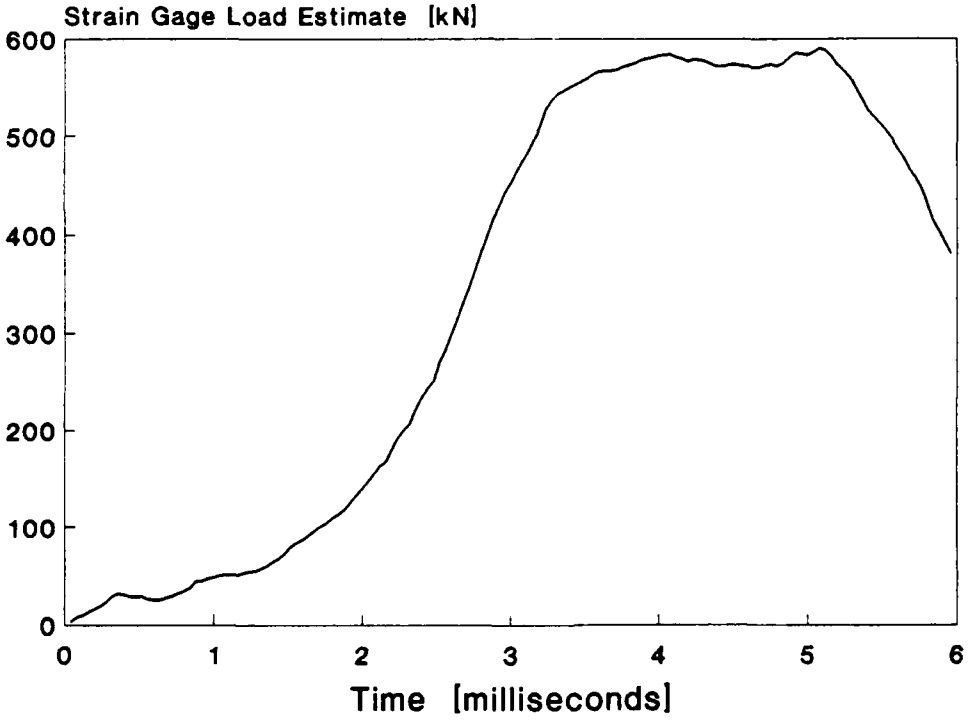

(b)

Figure 18: (a) Load line displacement vs. time and (b) load vs. time response of a shallow crack SE(B) specimen of the low hardening steel tested in a drop tower at 4.88 m/s.

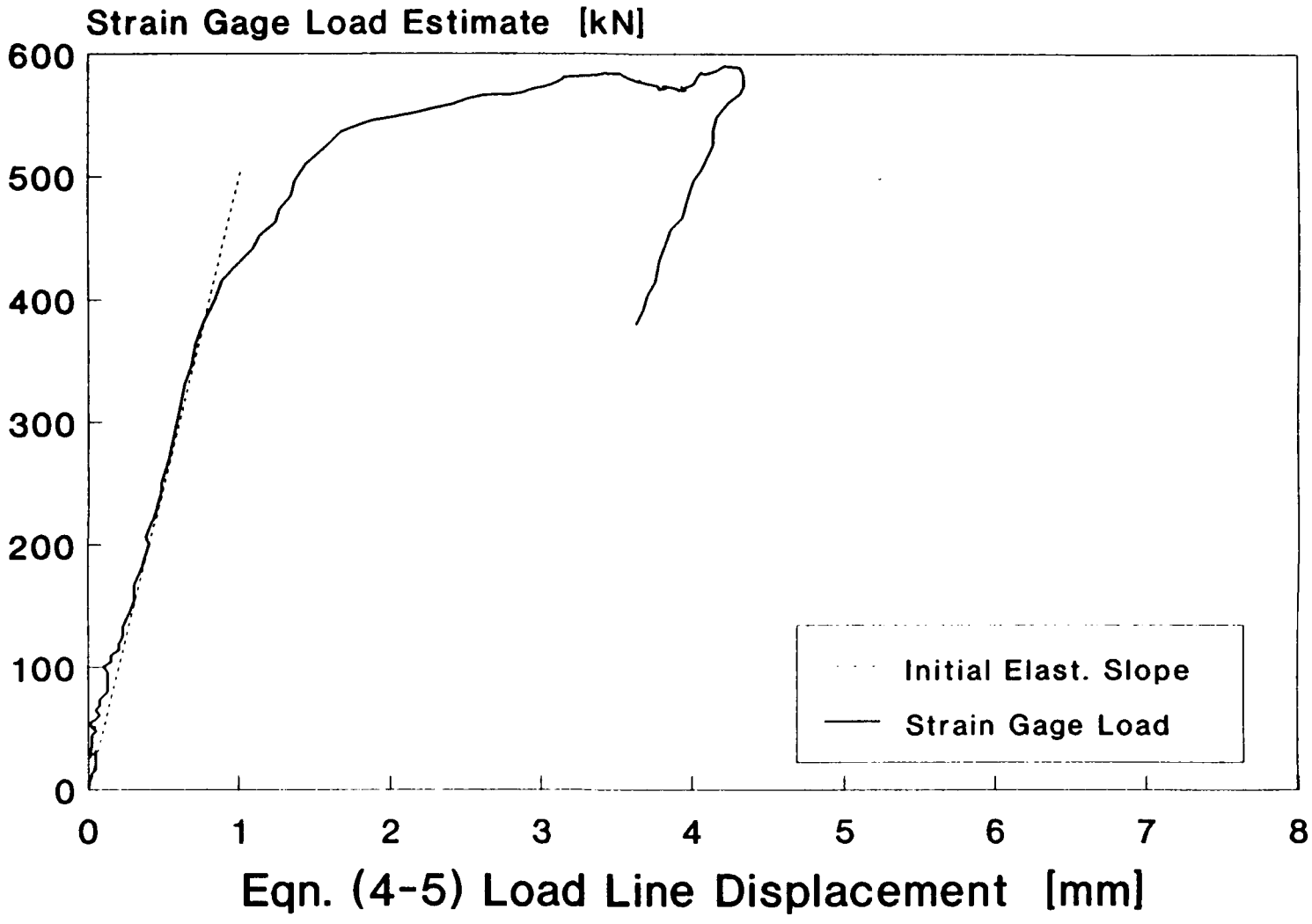

Figure 19: Load vs. load line displacement response of a shallow crack SE(B) specimen of the low hardening steel tested in a drop tower at 4.88 m/s.

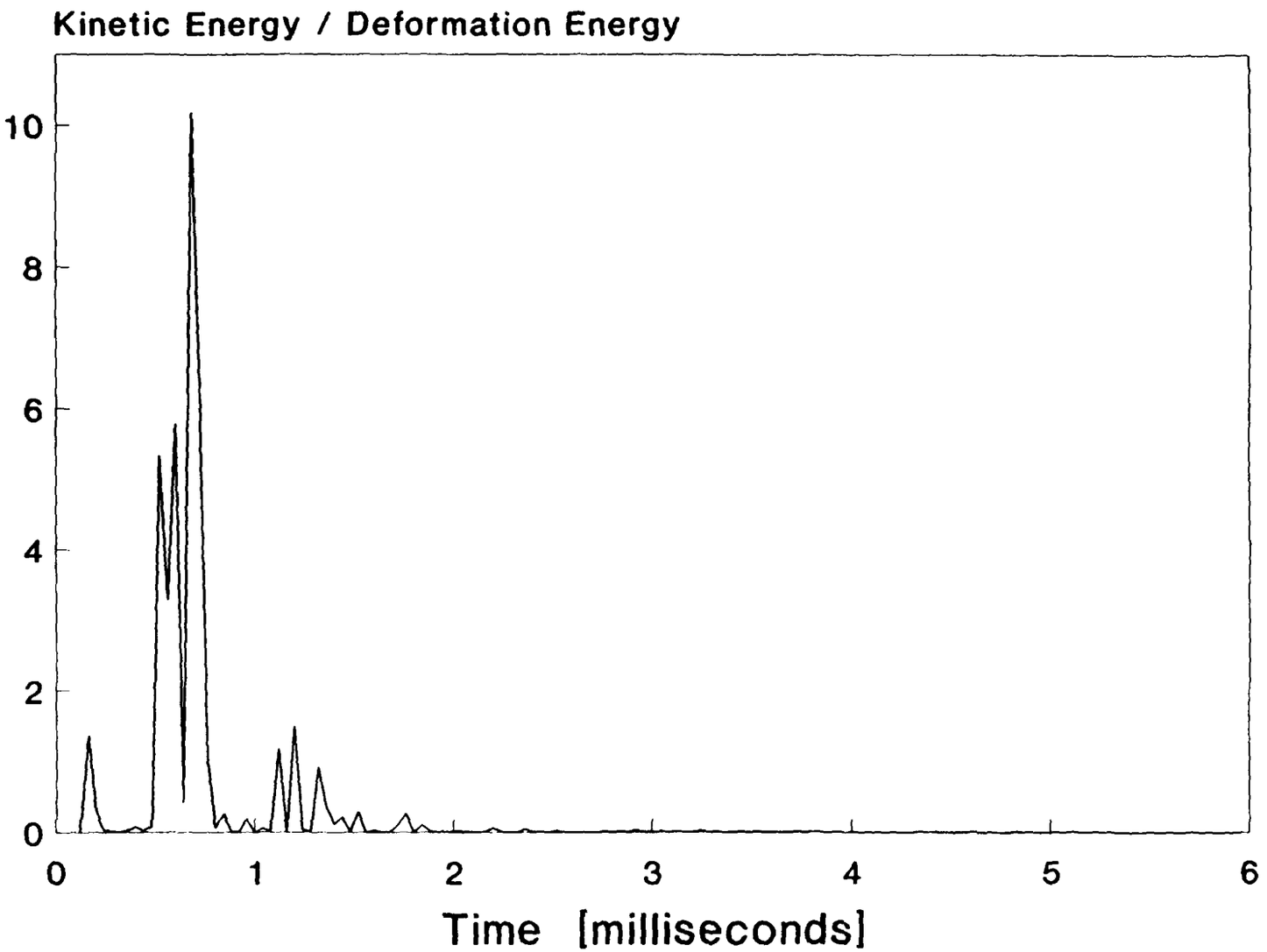

Figure 20: Variation of the ratio of kinetic energy to deformation energy with time in a shallow crack SE(B) specimen of the low hardening steel tested in a drop tower at 4.88 m/s.

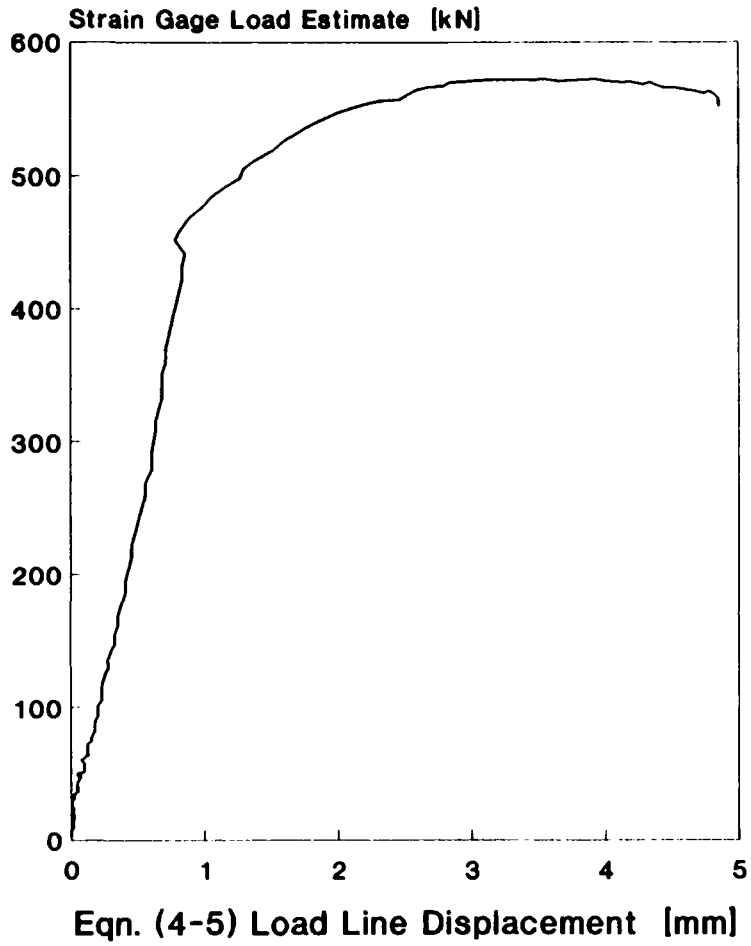

(a)

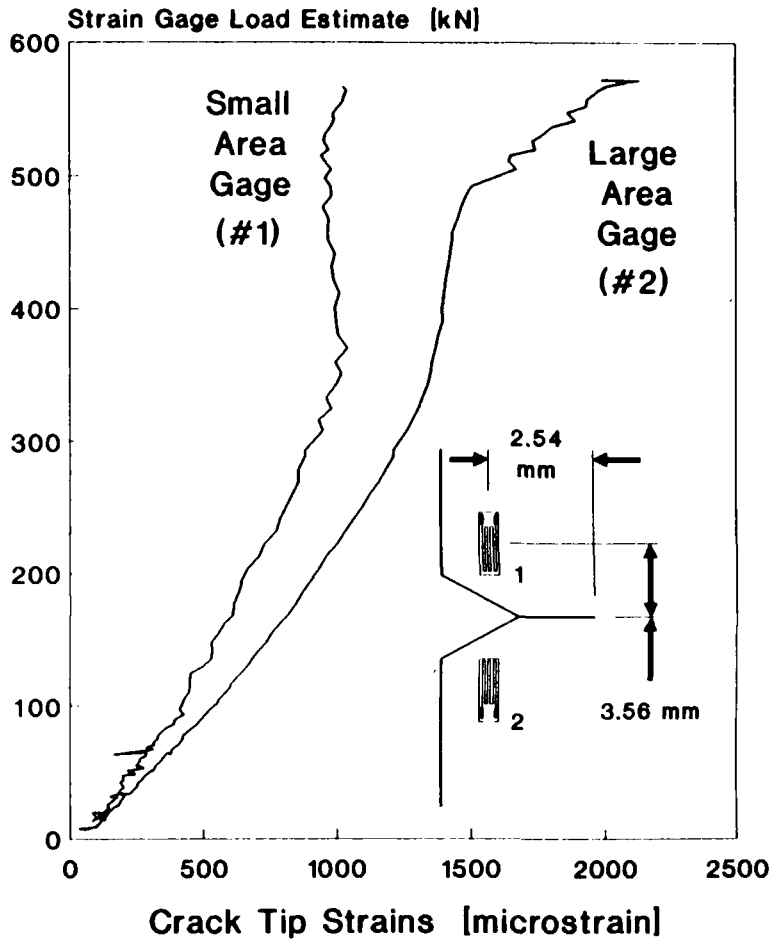

(b)

Figure 21: Test record from an impact SE(B) test of the low hardening steel which resulted in 4.70 mm of crack growth at the specimen midplane. (a) Load vs. load line displacement data, (b) Load vs. crack tip region strain.

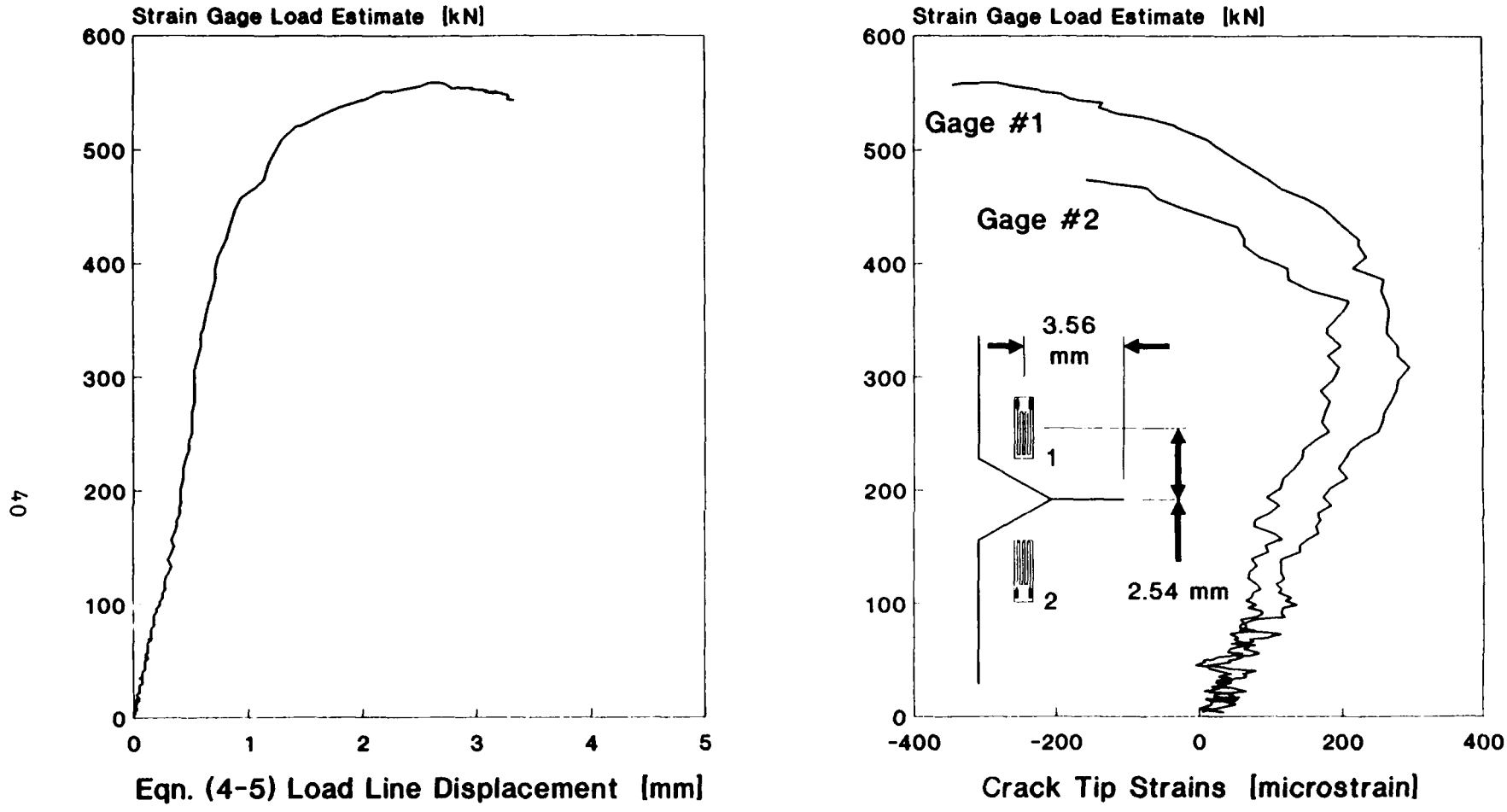

Figure 22: Test record from an impact SE(B) test of the low hardening steel which resulted in 1.52 mm of crack growth at the specimen midplane. (a) Load vs. load line displacement data, (b) Load vs. crack tip region strain.

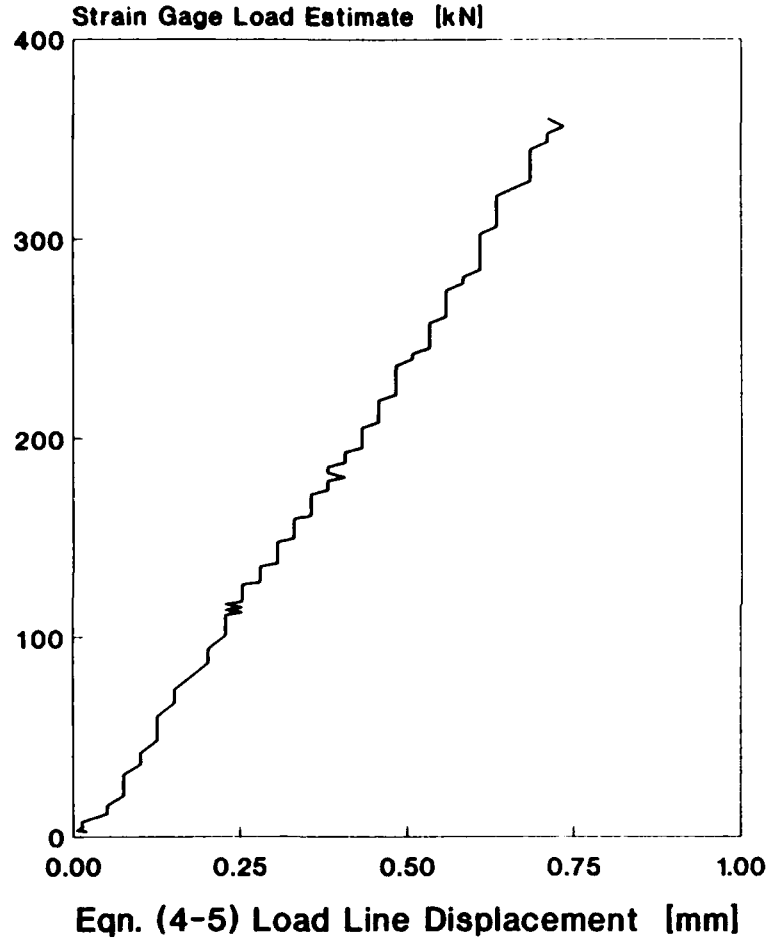

(a)

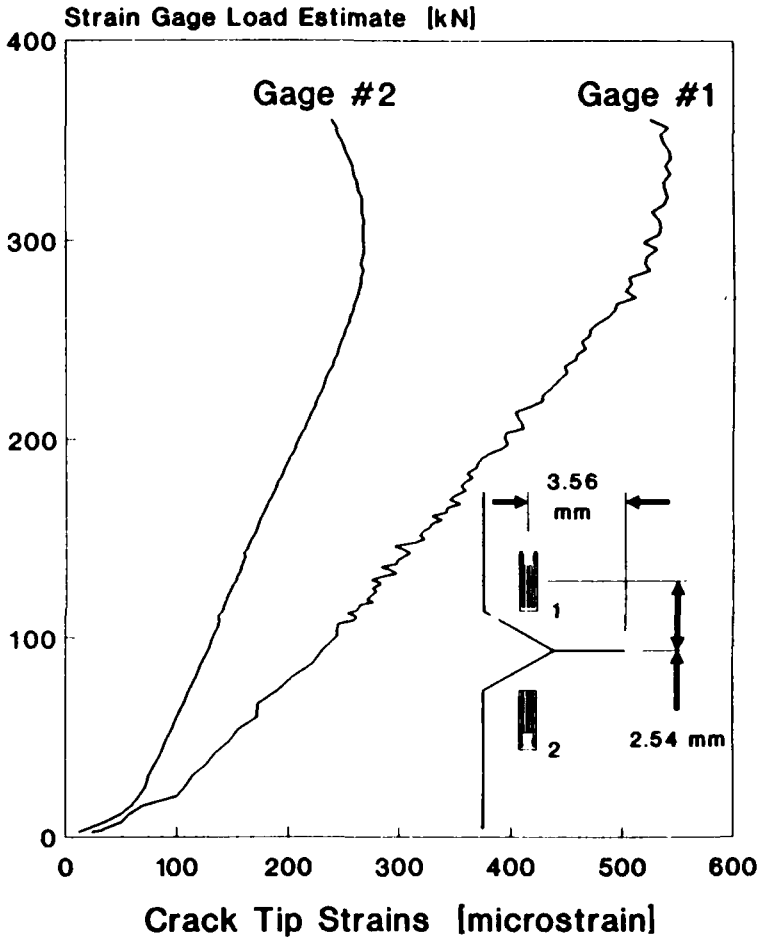

(b)

Figure 23: Test record from a quasi-static SE(B) test of the low hardening steel which did not result in macroscopically observable crack growth. (a) Load vs. load line displacement data, (b) Load vs. crack tip region strain.

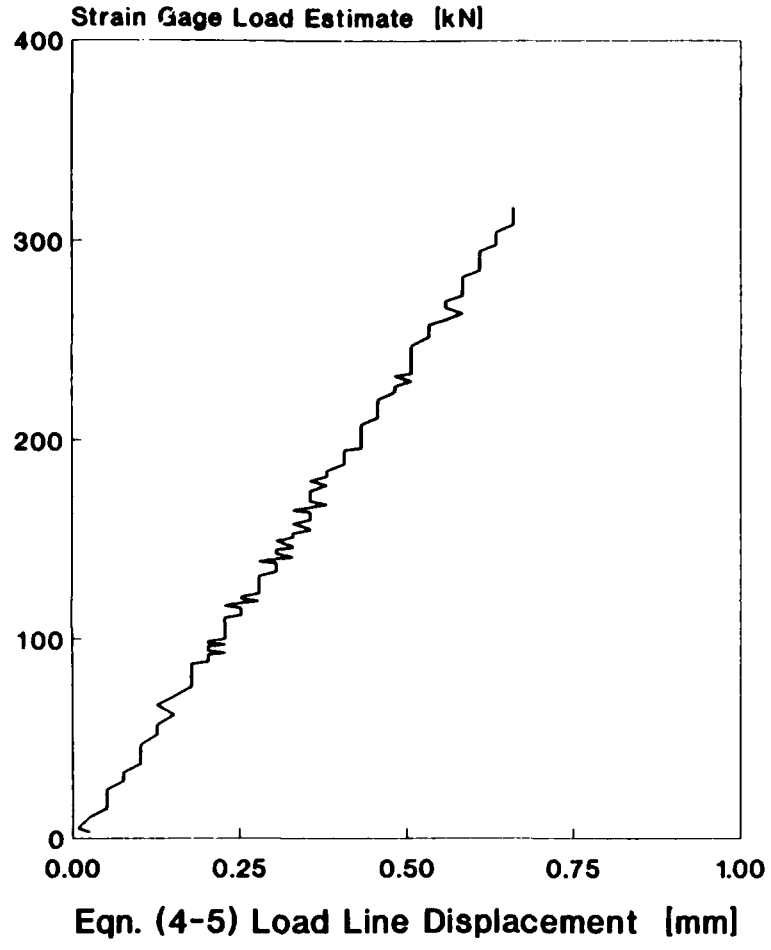

(a)

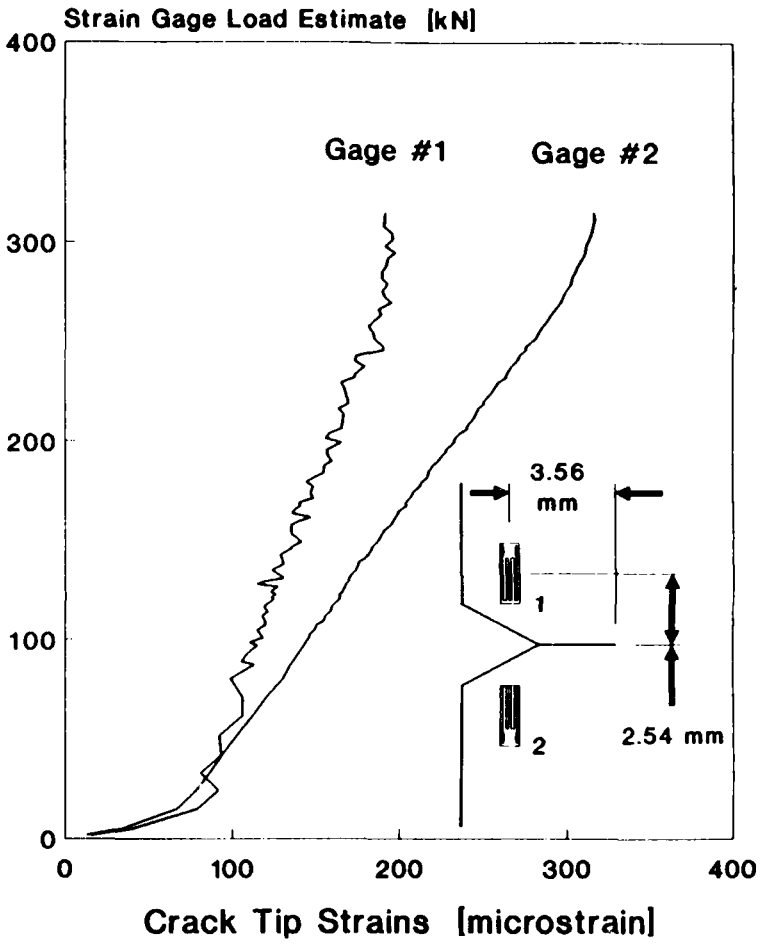

(b)

Figure 24: Test record from a quasi-static SE(B) test of the low hardening steel which did not result in macroscopically observable crack growth. (a) Load vs. load line displacement data, (b) Load vs. crack tip region strain.

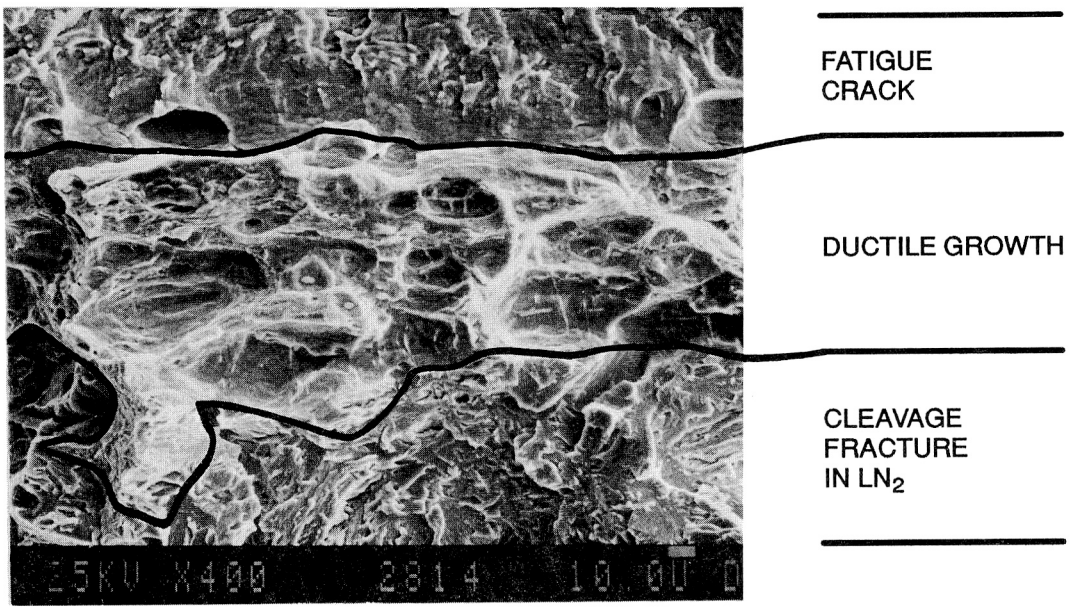

(a)

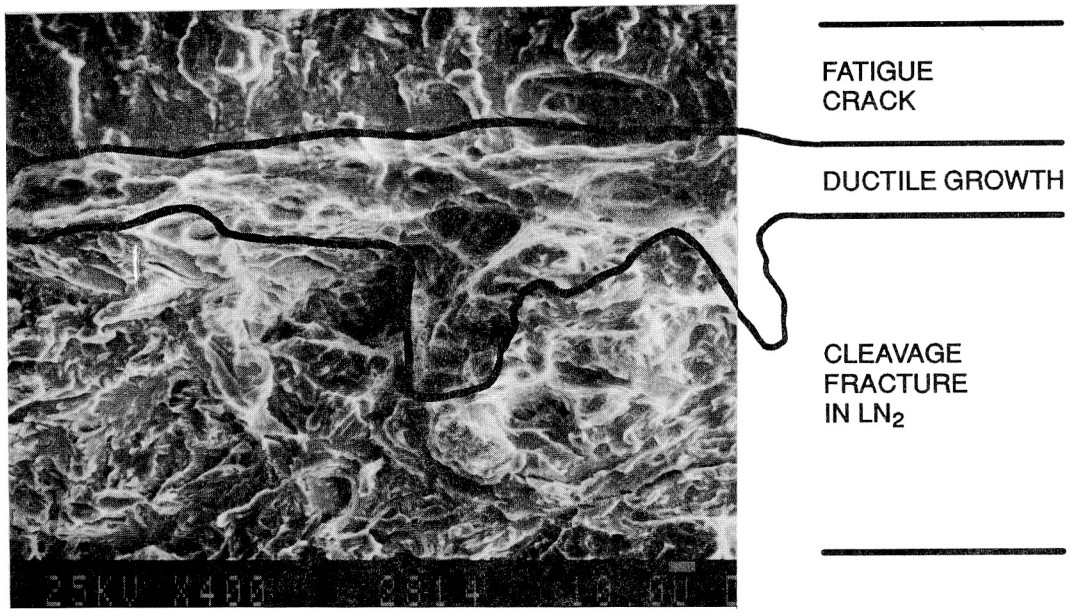

(b)

Figure 25: Microscopic ductile crack growth that resulted from the loading shown in (a) Figure 23 and in (b) Figure 24.

REFERENCES

[1] Sumpter, J.D.G., "Prediction of Critical Crack Size in Plastically Strained Welded Panels," *Nonlinear Fracture Mechanics: Volume II -- Elastic-Plastic Fracture, ASTM STP 995*, J.D. Landes, A. Saxena, and J.G. Merkle, Eds., American Society for Testing and Materials, Philadelphia, 1989, pp. 415-432.

[2] Kirk, M.T., and Hackett, E.M., "Fracture Behavior Prediction for Rapidly Loaded Surface Cracked Specimens," *Surface Crack Growth: Models, Experiments, and Structures, ASTM STP 1060*, W.G. Reuter, J.H. Underwood, and J.C. Newman, Jr., Eds., American Society for Testing and Materials, Philadelphia, 1990, pp. 121-151.

[3] Matsoukas, G., Cotterell, B., and Mai, Y.W., "Hydrostatic Stress and Crack Opening Displacement in Three-Point Bend Specimens with Shallow Cracks," Journal of Mechanics and Physics of Solids, Vol. 34, No. 5, pp. 499-510, 1986.

[4] Zhang, D.Z. and Wang, H., "On the Effect of the Ratio a/W on the Values of δ_i and J_i in a Structural Steel," Engineering Fracture Mechanics, Vol. 26, No. 2, pp.247-250, 1987.

[5] Matsoukas, G., Cotterell, B., and Mai, Y.W., "Crack Opening Displacement and Hydrostatic Stress," Department of Mechanical Engineering, University of Sydney, Sydney, Australia.

[6] Matsoukas, G., Cotterell, B., and Mai, Y.W., "The Effect of Shallow Cracks on Crack Opening Displacement," Engineering Fracture Mechanics, Vol. 24, No. 6, pp. 837-842, 1986.

[7] You, C.P. and Knott, J.F., "Effects of Crack Shape on Fracture Toughness in a High Strength Structural Steel," Engineering Fracture Mechanics, Vol. 24, No. 2, pp. 291-305, 1986.

[8] Sumpter, J.D.G., "J_c Determination for Shallow Notch Welded Bend Specimens," Fatigue Fract. Engng Mater. Struct., Vol. 10, No. 6, pp. 479-493, 1987.

[9] Sorem, W.A., et al, "An Analytical Comparison of Short Crack and Deep Crack CTOD Fracture Specimens of an A36 Steel, Presented at the ASTM 21st National Symposium on Fracture Mechanics held in Annapolis, Maryland on June 28-30, 1988.

[10] Madison, R.B., and Irwin, G.R., "Dynamic K_c Testing of Structural Steel," *Journal of the Structural Division, Proceedings of the American Society of Civil Engineers*, Vol. 100, No. ST7, July 1974, pp. 1331-1349.

[11] Joyce, J.A. and Hackett, E.M., "An Advanced Procedure for J-R Curve Testing Using a Drop Tower," *Nonlinear Fracture Mechanics: Volume I - Time Dependent Fracture, ASTM STP 995*, A. Saxena, J.D. Landes, and J.L. Bassani, Eds., American Society for Testing and Materials, Philadelphia, 1989, pp. 298-317.

[12] Hackett, E.M., Kirk, M.T., and Hays, R.A., "An Evaluation of J-R Curve Testing of Nuclear Piping Materials Using the Direct Current Potential Drop Technique," NUREG/CR-4540, August 1986.

[13] Joyce, J.A., "Application of Alternating Current Potential Difference to Drop Tower J-R Curve Measurement," NUREG/CR-4699, August 1986.

[14] Kirk, M.T. and Hackett, E.M., "An Evaluation of J-R Curve Testing Using Three-Point Bend Specimens," *Fracture Mechanics: Eighteenth Symposium, ASTM STP 945*, D.T. Read and R.P. Read, Eds., American Society for Testing and Materials, Philadelphia, 1988, pp. 347-373.

[15] Dodds, R.H., and Lopez, L.A., "Software Virtual Machines of Development of Finite-Element Systems," *International Journal for Engineering with Computers*, Vol. 13, pp. 18-26, 1985.

[16] Tada, H., Paris, P.C., and Irwin, G.R., The Stress Analysis of Cracks Handbook, Del Research Corp., 1973.

[17] Nakamura, T., Shih, C.F., and Freund, L.B., "Three-Dimensional Transient Analysis of a Dynamically Loaded Three-Point-Bend Ductile Fracture Specimen," *Nonlinear Fracture Mechanics: Volume I - Time Dependent Fracture, ASTM STP 995*, A. Saxena, J.D. Landes, and J.L. Bassani, Eds., American Society for Testing and Materials, Philadelphia, 1989, pp. 217-241.

INITIAL DISTRIBUTION

OUTSIDE CENTER

Copies	
1	DDRE/LIB
1	CNO/OP98T
3	ONCR
	1 0225
	1 4325
	1 Library
16	NAVSEA
	1 SEA 05M
	1 SEA 05M2 (Mitchell)
	1 SEA 05R
	1 SEA 55Y2
	1 SEA 55Y22 (Will)
	1 SEA 55Y23 (Nichols)
	1 SEA 55Y23 (Barbaro)
	1 SEA 55Y3
	1 SEA 55Y3 (Manuel)
	1 SEA 55Y3 (Sieve)
	1 SEA 55Y3 (Woods)
	1 SEA 55W3
	1 SEA 55W31
	1 SEA 55W31 (Robinson)
	2 SEA 99621
12	DTIC
1	NAVPGSCOL
1	USNROTCU
	NAVAMINU MIT
2	NRL
	1 Code 6380
	1 Code 6384

CENTER DISTRIBUTION

Copies		
1	011	
1	011.5	Caplan
1	172	Rockwell
1	1720.4	Wiggs
1	1720.4	Sickles
1	1720.4	Gifford
1	173	Beach
1	174	Hansen
1	28	Wacker
1	2801	Crisci
1	2801	Ventriglio
1	2802	Morton
1	2803	Cavallaro
1	2809	Malec
3	281	Gudas
3	2814	Montemarano
20	2814	Kirk
5	2814	Waskey
1	2814	Hackett
1	2814	R. Link
1	2814	Vassilaros
1	2814	Natishan
1	2814	L. Link
1	2814	Mikalac
1	2814	Koppenhoefer
1	2814	Jures
1	2814	Czyryca
1	2815	De Loach
1	2815	De Nale
1	283	Singerman
1	284	Fischer
1	522.1	TIC
1	5231	Office Services